Materials Today Sustainability 21 (2023) 100287

Contents lists available at ScienceDirect

Materials Today Sustainability

journal homepage: https://www.journals.elsevier.com/materials-today-sustainability

Photovoltaic efficiencies of microwave and Cu_2ZnSnS_4 (CZTS) superstrate solar cells

S.T. Yussuf*, K.C. Nwambaekwe, M.E. Ramoroka, E.I. Iwuoha**

Key Laboratory for NanoElectrochemistry, 4th Floor Chemical Sciences Building, University of the Western Cape, Robert Sobukwe Road, Bellville 7535, Cape Town, South Africa

ARTICLE INFO

Article history:
Received 30 September 2022
Received in revised form
11 November 2022
Accepted 30 November 2022
Available online 7 December 2022

Keywords:
Kesterite solar cell
Microwave synthesis
Nanomaterial
Superstrate configuration
Thin-film

ABSTRACT

Organic and inorganic materials such as perovskites, copper indium gallium diselenide, cadmium telluride, and copper zinc tin sulfide/selenide (CZTS/Se) have been employed to capture unlimited sunlight through the photovoltaic effect. CZTS/Se is regarded as the most promising, most environmentally friendly, most abundant candidate with high absorption coefficient and tunable bandgap for the generation of solar energy. Superstrate architectures have numerous advantages over the substrate architectures and for this reason; it offers a promising route for producing solar cells at a relatively low cost. This article reviews the state-of-the-art knowledge on the synthesis, crystal structure, electronic properties, defects, and secondary phases of CZTS. The CZTS solar cell device architecture and mechanism of the substrate and superstrate configurations were also covered in the review. The preparation of superstrate CZTS via vacuum and non-vacuum methods, as well as their photovoltaic efficiencies were critically discussed. The microwave synthesis and characterization of CZTS nanoparticles were also reviewed with respect to the effect of temperature, surfactant, and reagents on the physical properties of the nanomaterials. The application of microwave-synthesized CZTS nanoparticles in the advancement of thin film solar cells was also critically examined. Finally, the challenges and the prospects of CZTS solar cells were also presented.

1. Introduction

The use of energy is vital to the economic growth, social development, technological advancement, and better living conditions in developed, developing, and underdeveloped countries in the world. There are basically three sources of energy: renewable, fissile, and fossil. The fossil sources include natural gas, coal, petroleum, oil shales and tar sands; the renewable includes but not limited to solar, hydropower, biomass, wind, and geothermal, while the sources of fissile energy are thorium and uranium [1–3]. Energy demands and consumption is expected to skyrocket in the near future due to rise in the population and increase in standard of living. It is expected that the demand on fossil fuels will also increase as more than 85% of the world's total energy is generated by fossil fuels, which is a finite source [4,5]. The combustion of fossil fuels is inextricably linked to global warming due to the high emission of greenhouse gases (CO_2, methane, and other gases), which have dreadful consequences on the environment and human lives [6,7]. In addition, energy produced from fossil fuels is becoming more expensive and it is at the verge of being scarce in the coming future. As a result, it is critical to intensify research into alternative energy sources that can help manage rising energy demand while also lowering CO_2 emissions [6,7]. Due to its infinite supply, cleanliness, sustainability, reproducibility, and ability to be replenished quickly, renewable energy is the only source that can address the world's energy problems [2,7,8]. The search for alternatively renewable, clean, inexhaustible, and primary sources of energy that can tackle the growing energy demand and reduce environmental pollution is important. Solar energy is currently the only renewable energy source that can completely replace conventional energy sources because it is the most abundant, most promising, cost-effective, scalable, flexible, and efficient of all renewable energy sources [9–11]. Solar photovoltaic (PV) has been predicted to be the largest source of renewable energy by 2040 with a production capacity of about 25.1% out of the global power

* Corresponding author.
** Corresponding author.
E-mail addresses: 3773164@uwc.ac.za (S.T. Yussuf), eiwuoha@uwc.ac.za (E.I. Iwuoha).

https://doi.org/10.1016/j.mtsust.2022.100287
2589-2347/

generation [12–14]. Several PV technologies, including thin film, organic, and wafer have been thoroughly studied to achieve high efficiency, cost-effectiveness, and reliability. Silicon-based solar cell devices are desirable owing to their availability, robustness, high efficiency, and compatibility with microelectronics technology. However, due to the low absorption of Si, silicon-based technology consumes a lot of material (~100 μm); the price of processing c-Si solar cells is on the high side and also involves complicated procedures such as ion implantation and high-temperature treatment which hinders the effective competition with fossil energy [15]. Thin-film PV technologies satisfy the minimum material usage, low manufacturing costs, and high efficiency requirements, which are some of the major factors that need to be met in order to generate power at a relatively low cost and enable high penetration of solar energy in the market. Essentially, copper indium gallium diselenide/disulfide (CIGS), cadmium Telluride (CdTe), amorphous silicon (a-Si), and copper indium diselenide/disulfide (CIS) are the only thin films commercially available from which only CIGS and CdTe have reached a power conversion efficiency (PCE) of above 20% [16]. Nevertheless, the toxicity of cadmium and telluride, the rarity and high cost of indium have hindered these technologies for large-scale production, and this has contributed to the hunt for novel earth-abundant and environmentally safe semiconductor materials for PV applications [17–25]. In the PV research community, quaternary Kesterite-structured tetrahedral semiconductors such as Cu_2ZnSnS_4 (CZTS), $Cu_2ZnSnSe_4$ ($CZTSe_4$), and $Cu_2ZnSn(S_x,Se_{1-x})_4$ have become the most auspicious semiconductor active-layers for affordable thin-film solar cell (TFSC) applications due to their abundance in nature, low toxicity, excellent absorption capabilities, direct bandgaps, and high theoretical efficiency [26–34]. Various synthetic routes to kesterite thin films are available in the literature, and it includes both vacuum-based or physical deposition techniques and non-vacuum-based or chemical techniques. The most commonly used vacuum based is sputtering and co-evaporation, and it uses highly expensive vacuum equipment, consumes a lot of energy, which makes it unsuitable for industrial-scale applications, while non-vacuum techniques are beneficial for scalability and economic viability because they do not make use of vacuum, do not require high temperatures, provide relatively homogeneous films, ease of preparation, and the use of small materials. It includes hot injection, sol-gel, electrodeposition, hydrothermal, solvothermal, nanocrystal dispersion, hydrazine-based deposition, spray pyrolysis, chemical bath deposition (CBD), microwave, and other pure-solution methods. The highest efficiency for CZTSSe is 12.6%; it is currently the champion of CZTSSe solar cell and was fabricated by highly toxic and flammable hydrazine-based solution method by International Business Machines (IBM) solar cell, which makes it non suitable as a source of green energy [26,35–45]. In the field of nanomaterials synthesis, microwave is beginning to see a huge surge as it provides an alternative uniform heating source that allows for the realization of chemical reactions at shorter times, faster reaction speed, side reaction suppression, increases yield, and is highly reproducible compared to the traditional laboratory heating methods, which is usually carried out for days or hours thereby leading to a reduction in price, saving energy, and improves the materials production efficiency [46–50].

Majority of CZTS solar cell devices have been developed with the architecture of Mo/absorber-CZTS/buffer/metal oxide nanostructures/metal electrodes, and it has been shown that these configurations have some drawbacks including the degradation of the metal oxide caused by the thermally unstable absorber layer resulting to the creation of buffer interfaces. Furthermore, the reaction between the molybdenum (Mo) back contact and CZTS leads to corrosion and instability of the surface of CZTS throughout the heating temperature. A potential way to mitigate the above problems is by introducing a superstrate architecture in CZTS solar cells by directly depositing the metal oxide on the substrate, which is then preceded by annealing at a higher temperature in order to avoid the direct contact between the CZTS and the conducting substrate [51]. Combining the advantages of nanostructures with a thin film has been shown to increase the conversion efficiencies of thin film solar devices and metal oxide nanostructures due to their controllable dimensions and aligned morphologies have been shown to generate, collect, and transfer charges efficiently as a result of the large junction area and the short collection distance from the interface [52]. This review aims to discuss some of the properties of CZTS. Insights into device architecture in both the substrate and superstrate will be discussed. The different fabrication techniques of CZTS absorber materials in the superstrate configuration will be reviewed. The effect of parameters such as concentration, surfactant, and temperature on microwave-synthesized CZTS nanoparticles as well as their PV efficiencies will also be discussed.

2. Kesterite

2.1. Crystal structure

Kesterite with the formula $Cu_2(Zn, Fe)SnS_4$ is a dense, green-black, or black sulfide mineral. The zinc-rich form is called kesterite, and the zinc-poor form is called ferrokesterite or stannite. It is sometimes called isostannite because of their similarities [53]. In the literature, kesterite abbreviated as CZTS is referred to as the sulfide, selenide, or sulfide-selenide form of the material. It is a quaternary compound with the configuration I_2–II–IV–VI_4 derived by substituting indium with equal amount of zinc and tin in $CuInS_2$ ternary compound (Fig. 1) but still maintaining the charge neutrality and the overall valence state of the compound [54]. CZTS/Se can exist in three tetragonal crystal structures: stannite (space group I42), kesterite (space group I4), and primitive-mixed CuAu (PMCA) (space group P42 m) as shown in Fig. 2 [55–58]. Kesterite (KS) is derived from group I-III-IV_2 chalcopyrite (CH) structure, while stannite (ST) and PMCA are both formed from group I-III-IV_2 CuAu-like (CA) structure [56]. Kesterite (KS) and stannite (ST) are both body-centered tetragonal where c = 2a, whereas the structure of the PMCA is primitive tetragonal with c-a. The three fundamental structures differ in the way the metal cations are arranged and stacked within the tetrahedral voids. In KS, two of the three cation layers alternate each consisting of Cu and Sn or Cu and Zn, whereas in PMCA and ST structures, one of the Cu layers alternates

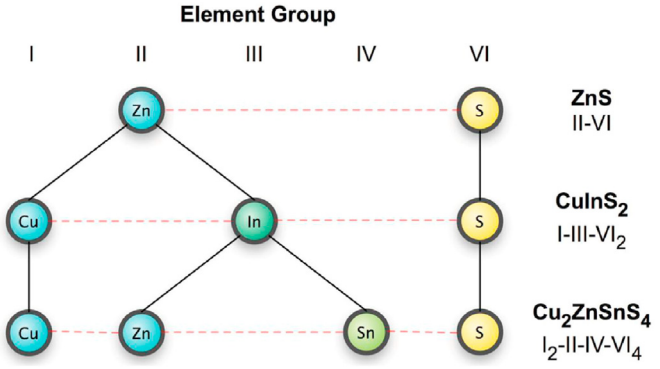

Fig. 1. Ternary, quaternary, and binary semiconductors relationship leading to the formation of Cu_2ZnSnS_4 beginning with the parent compound II-VI. [Copyright with permission from John Wiley & Sons] [54].

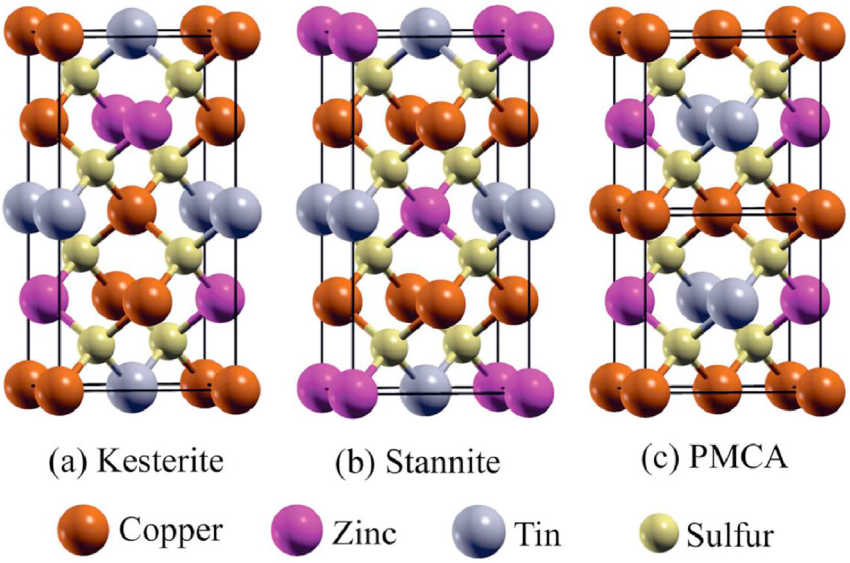

Fig. 2. Kesterite, stannite, and PMCA structures for CZTS/Se. [Copyright with permission from American Institute of Physics] [58].

with one of Zn and Sn layer [58]. Studies have shown that kesterite (KS) is more thermodynamically stable compared to stannite (ST) and primitive-mixed structures due to smaller strain energy, lower Madelung energy, larger bandgap, and more negative coulomb energy [56]. Computational studies show that KS is only about few meV (about 3 meV/atom) lower in ground energy state per formula unit than the ST and PMCA, which may be indicative of the coexistence of these structures in synthesized samples [56]. CZTS/Se materials have been shown to experimentally crystallize in either KS or ST structures, while PMCA is yet to be observed experimentally [56,58]. Using X-ray diffraction (XRD) technique to distinguish between these structures is very difficult as Cu^{+} and Zn^{2+} are isoelectronic and due to the interaction of X-rays with the atoms' electron shells [59]. Due to the disparity in neutron scattering lengths of copper ($b_{Cu} = 7.718(4)$ fm) and zinc ($b_{Zn} = 5.680(5)$ fm) [60,61] synchrotron, neutron diffraction X-ray, and Raman spectroscopy [58] have been used to distinguish between these structures. However, because Cu and Zn are practically randomly positioned, there is still no agreement on the real structure of CZTS/Se [55].

2.2. Electronic band structure

The electrical properties, such as the energy band width, doping behavior, transport properties, and density of states, are of utmost importance for considering a material as an absorber for PV applications [59]. The CZTS/Se bandgap is usually determined experimentally by investigating the absorption spectra or reflection spectra at the place where a straight line intersects the abscissa axis, through extrapolation [53]. Details of the electronic band structures of CZTS/Se are well reported by Persson in 2010 [62]. The result showed that CZTS and CZTSe electronic band structures have similar band structures with direct energy gaps of Γ-point as shown in Fig. 3. The estimated energy gap (*Eg*) for kesterite (CZTS) is 1.56 eV; for stannite (CZTS), it is 1.42 eV; for kesterite (CZTSe), it is 1.05 eV; and for stannite (CZTSe), it is 0.89 eV. The above values are in agreement with vast majority of investigations on the CZTS bandgap, which is calculated to be close to 1.5 ± 0.01 eV irrespective of the methods used for the determination of bandgap, and for the CZTSe bandgap, there are huge discrepancies among the reported values. The bandgap reported for CZTSe can be categorized into two groups, around 1 eV and 1.5 eV, respectively. The explanations for the discrepancies is difficult to ascertain due to the combination of several complex methods of preparation and dissimilar methods of determining the bandgap [27,53,62–73]. However, two interesting points were made by Ahn et al. [74] in their study. The first was that the bandgap of 1.5 eV only resulted from transmission measurements, while the bandgap of 1.0 eV resulted from other procedures such as photoluminescence, external quantum efficiency (EQE) of the completed device, and the theoretical calculations. The second point made is that majority of researchers analyzed their samples using only XRD method as the only phase identification technique, which may not be able to detect the existence of secondary phases like ZnSe and Cu_2SnSe_3 [74]. In view of the points mentioned above, it was concluded that the key explanations for the variations between the *Eg* values may be attributed either to the different methods used in the determination of bandgaps or to the existence of secondary phases, which can be difficult to detect by the use of powder XRD. Subsequent research carried out showed that the explanation of the first scenario was impossible since all CZTSe samples with single phase were characterized by $Eg \approx 1.0$ eV regardless of the technique used to evaluate the bandgap while examining CZTSe samples co-existing with secondary phases exhibited distinct discrepancies in the bandgap (*Eg*) values of the films generated at dissimilar temperatures of the substrate. Most importantly, in the final samples, as the temperature of the substrate increases, tin content reduced and the ZnSe secondary phase was formed. The overestimated *Eg* values of the CZTSe films are as a result of the micro inclusions of ZnSe [53].

2.3. Defects

The presence of four or more elements in CZTS/Se compared to ternary and binary semiconductors leads to an improvement in the flexibility of the material properties. Consequently, it is expected that a wide variety of inherent lattice defects will be formed having a major impact on optical, electrical, and PV properties. Vacancies, antisites, interstitials, and complexes/clusters are some of the defects formed. The defect complexes/clusters and defects form shallow acceptor levels, shallow donor levels, deep trap states, and

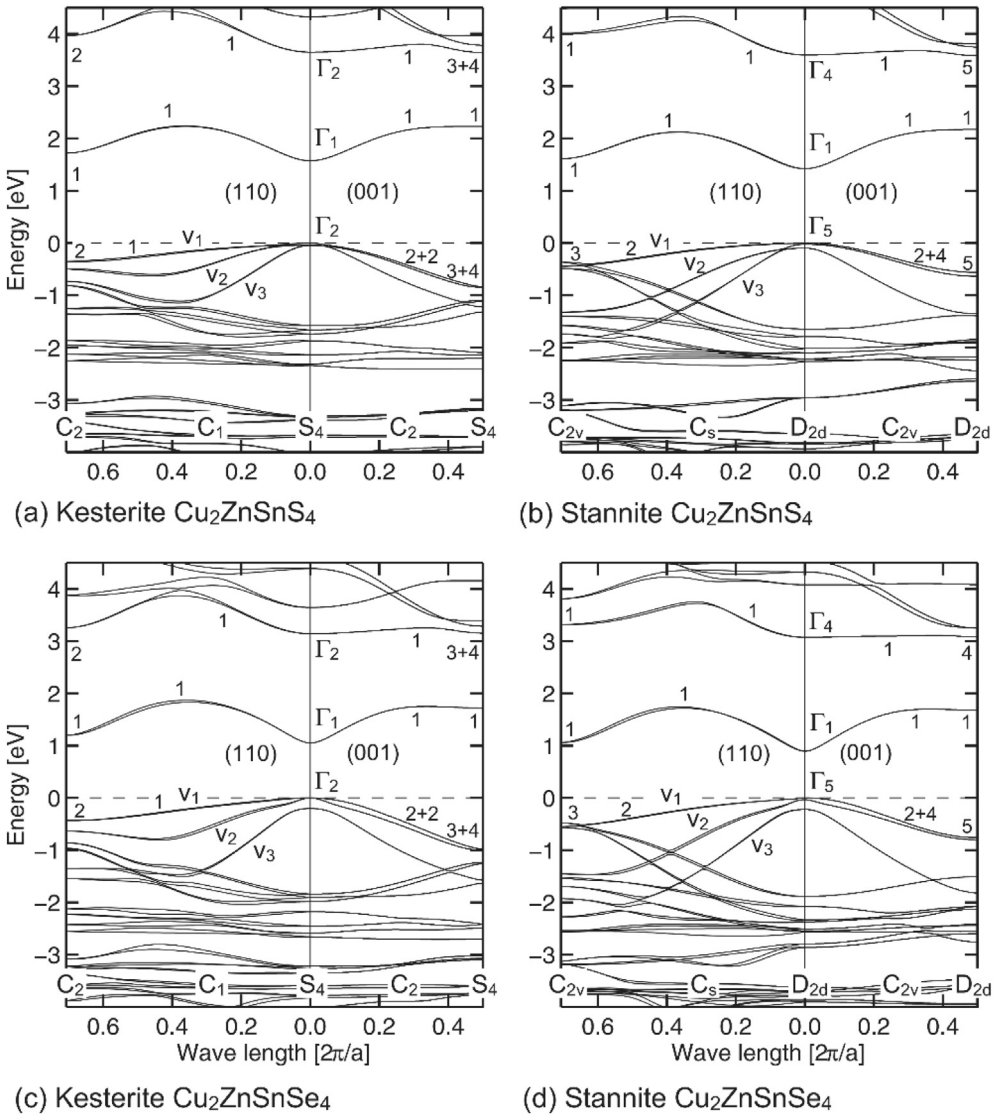

Fig. 3. Electronic band structure of kesterite and stannite CZTS and CZTSe formations along symmetry axes 110 and 00 [Copyright with permission from American Institute of Physics] [62].

mid-gap states in the bandgap of CZTS materials thereby influencing its optoelectronic properties [75,76]. Fundamentally, during the growth of CZTS/Se thin film/bulk crystals, thirteen likely isolated intrinsic point defects can form in kesterite structure, and they are vacancies (V_{Sn}, V_{Zn}, V_S, and V_{Cu}), antisites AB where element A replaces element B (Cu_{Sn}, Cu_{Zn}, Zn_{Sn}, Zn_{Cu}, Sn_{Zn}, and Sn_{Cu}), and interstitial defects (Sn_i, Zn_i, and Cu_i). In addition to these defects, the defects in the donor and acceptor may make up for and attract one another, thereby creating defect complex/clusters ($Zn_{Sn} + 2Zn_{Cu}$, $V_{Cu} + Zn_{Cu}$, $2Cu_{Zn} + Sn_{Zn}$). Chen et al. [75] evaluated the formation energies of several lattice defects in CZTS/Se quaternary compound as shown in Fig. 4 and came to two conclusions that (i) the energies of formation of most acceptor defects is less compared to that of donor defects, which explains the *p*-type conductivity observed experimentally and suggests that *n*-type doping may be problematic in these compound (ii) Cu_{Zn} antisite is the defect with the lowest energy (i.e., for the assumed chemical potentials), which is different from that of $CuInSe_2$ where Cu vacancy is the dominant defect. The estimation of the ionization levels of point defects in the Cu_2ZnSnS_4 bandgap as derived in Fig. 3 and are shown as vertical plots more visibly in Fig. 5. A number of authors have used density functional theory (DFT) and first principle calculations to examine the defects mechanism and energies of formation of various potential point defects in kesterites. Cu_{Zn} antisite is the acceptor with lowest formation energy in CZTS. Other acceptor defects are only slightly higher than those of the dominant Cu_{Zn} like V_{Cu}, V_{Zn}, Zn_{Sn} and Cu_{Sn} formation energies and are therefore predicted to be present in lower concentrations. In contrast to an acceptor level that is 0.02 eV higher than the VBM for the V_{Cu} defect, the Cu_{Zn} defect has an acceptor level that is 0.12 eV higher than the valence band maximum. The deeper Cu_{Zn} level can lead to high defect concentrations that maybe harmful to the maximum efficiency of the solar cell. Copper-poor growth can lead to higher V_{Cu} concentrations, which have been experimentally shown to improve performance [32,54,76–79].

2.4. Secondary phases

Due to the existence of four or even five elements in CZTS/Se, the possibilities for the formation of secondary phases are higher than

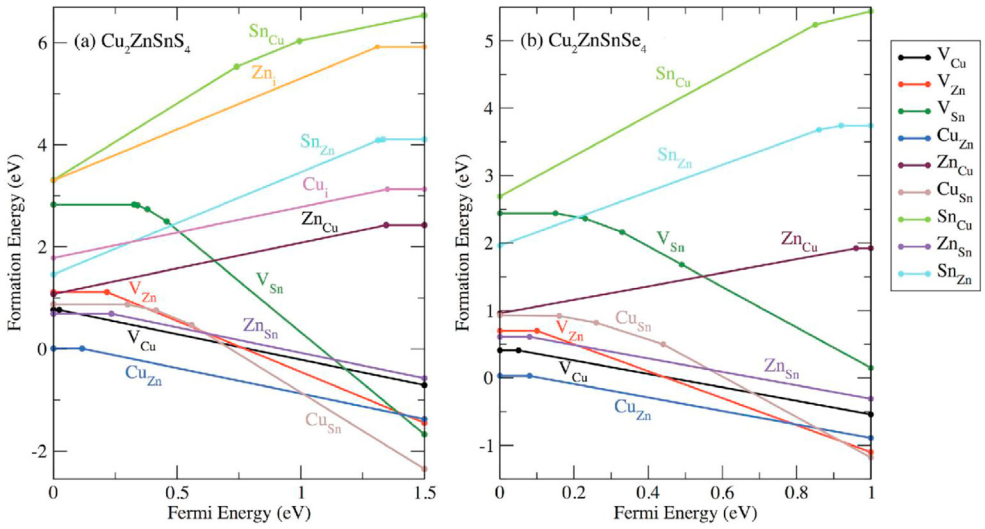

Fig. 4. Formation of lattice defects energy calculated as a function of Fermi energy at the thermodynamic chemical-potential point for (a) Cu_2SnZnS_4 (b) $Cu_2SnZnSe_4$. [Copyright with permission from John Wiley & Sons] [54].

those of ternary semiconductors [80]. Olekseyuk et al. [81] showed that a single CZTS phase occurs at growth temperatures of approximately 550 °C within a relatively tiny region of the phase diagram. Such narrow-phase stability makes it easy to form defects and secondary phases during and after growth processes. Fig. 6 depicts the pseudo-ternary phase diagram for CZTS phase formation and additional secondary phases as well as their crystal structures. The secondary phases include ternary CuSnS/Se, binary ZnS/Se, CuS/Se, and SnS/Se compounds, and it has been discovered and reported by several authors [76,82,83]. It has been shown experimentally that the best devices with higher efficiencies are prepared under Cu-deficient and zinc-rich conditions. Among these secondary phases, zinc sulfide (ZnS) and copper tin sulfide (CTS) have relatively small enthalpies of formation. Secondary phases may exist at the interface whether surface and back contact or may be present in the bulk, and some studies have reported their existence across the entire film's thickness. The negative impacts of the secondary phases cannot be prevented when it exists in the back region or in the bulk, and the only likely solution is in prevention, by selecting idealized conditions for synthesis, selecting the right precursors, Cu-poor composition, optimum process parameters, and post-heat treatments. Equally, when it exist on the surface, etching is a common method to remove them [76,82,83]. The bandgap of the secondary phases can tell us how harmful a secondary phase will be to the performance of a solar cell. If the secondary phase bandgap is lower than that of the actual absorber, the open circuit voltage of the PV cell will be reduced. In the sulfide system, CuS, CTS, and SnS have lower bandgap, while in the selenide system, only CTSe has a low bandgap, indicating that secondary phases are less harmful in the selenide kesterite absorbers than in the sulfide absorbers. Secondary phases that have higher bandgaps are much less harmful, but when present in large amounts, they can obstruct transport or at least increase series resistance [84].

3. CZTSSe deposition techniques

Various synthetic routes to kesterite thin films are known and they can be grouped into vacuum-based deposition or physical techniques and non-vacuum based or chemical techniques.

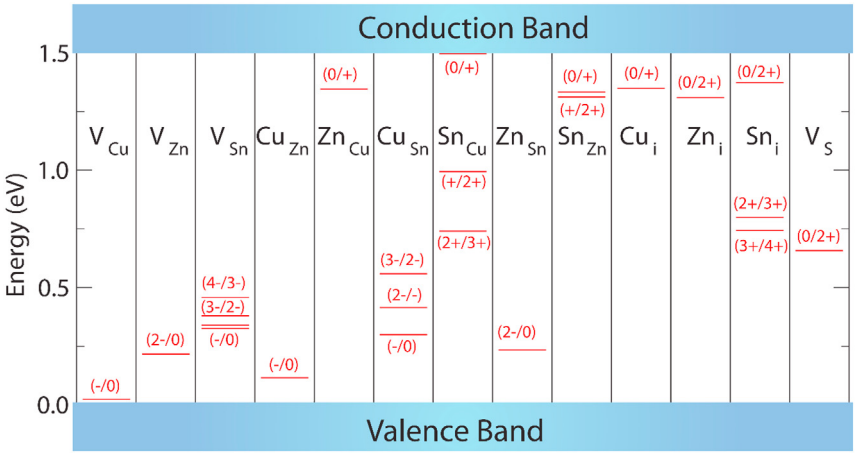

Fig. 5. Intrinsic defect ionization levels in the Cu_2ZnSnS_4 bandgap. The copper vacancy produces a shallow acceptor level directly above the valence band, but the Cu-on-Zn antisite produces an energy level that is 0.12 eV higher [Copyright with permission from John Wiley & Sons] [54].

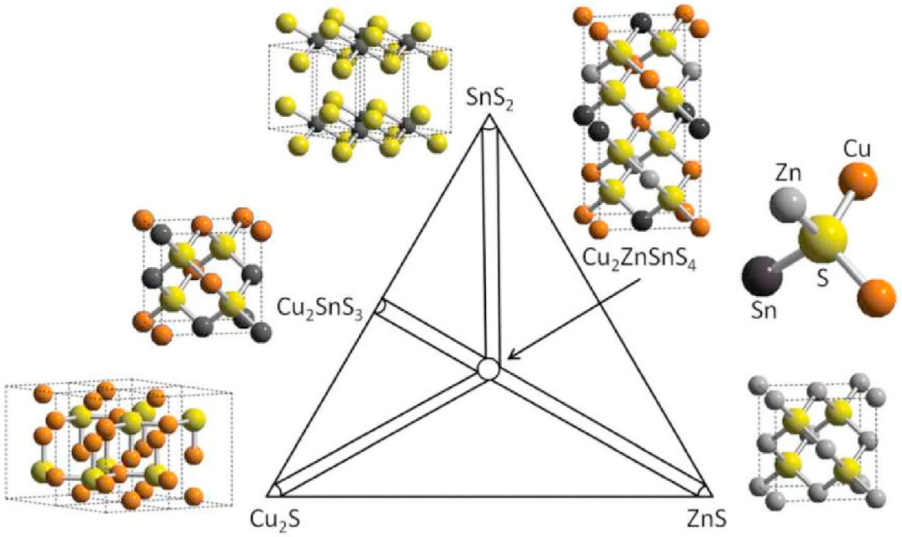

Fig. 6. The pseudoternary phase diagram used to generate the phase of CZTS, various secondary phases, and the crystal structures. [Copyright with permission from The Royal Society of Chemistry] [76].

3.1. Vacuum techniques

It can be grouped into a single or a two-step vacuum process. In the single-step process, all the constituents elements are simultaneously incorporated, while in the two-step process, the incorporation of the precursors takes place employing a process that involves an ambient temperature such as sputtering [85–88] or evaporation [89,90] followed by high temperature annealing [89,91–95]. The chalcogens may be added into the precursor [96,97] or during the annealing process [92,93,95,98,99] by sulfurization [90,99,100] or selenization [96,97].

The advantages of vacuum techniques include high uniformity, greater prospects for producing high-quality thin film devices, simple control over the chemical composition of the thin film, and good reproducibility. The most commonly used is sputtering and co-evaporation and others include pulsed laser [101] and chemical vapor deposition [102]. Vacuum-based techniques suffer from low throughput, high material utilization, high energy consumption and use highly expensive vacuum equipment which makes it unsuitable for large-scale production [103].

3.2. Non-vacuum-based techniques

The advantages of this technique over the vacuum-based technique include ease of production, use of minimal materials, low temperature requirement, exclusion of high vacuum equipments and provide relatively homogeneous films making it suitable for scalability and viable industrial development [44,103]. It includes hot injection, sol-gel, electrodeposition, hydrothermal, solvothermal, nanocrystal dispersion, hydrazine-based, microwave, spray pyrolysis, CBD, and other pure-solution methods [37,104–127]. The world record for any CZTSSe solar cell has been stalled at 12.6% using a non-vacuum hydrazine solution-based approach [128]. Hydrazine being highly toxic and highly explosive makes it an unrealistic approach to an environmentally friendly solar cell materials capable of competing with the conventional silicon solar cell. Recently, a certified efficiency of about 13% was achieved via eco-friendly solution-based approach, demonstrating promising solar cell application prospects, and it is currently the best efficiency reported for CZTSSe solar cells [129]. Among the different non vacuum techniques, microwave irradiation is a well-established approach for the controlled synthesis of various nanomaterials because it has a number of advantages over other methods. Some of these benefits include enhanced homogeneity, faster crystallization time, higher yield, better size control, high purity, and reproducibility [130].

4. Basic structure of a typical CZTS/Se solar cell

The most widely used architecture of CZTS/Se is a complex multilayer module composed of glass or a flexible polymer substrate, which serves as an electrode layer's support that is typically molybdenum (Mo) films with a thickness of a few 100 nm [53,131], a soda-lime glass is common for CZTS/Se solar cells as it helps diffuse sodium through the molybdenum, further aiding the growth of larger particles in CZTS absorber material [132,133] and in some cases, ITO/FTO are used [52,134]. Generally, the Mo is usually deposited on the substrate by sputtering. Due to its low resistivity and stability, Mo acts as the back contact, and it assists in the formation of a molybdenum disulfide (MoS_2) layer, which is beneficial for ohmic contact with the CZTS layer. Owing to its smaller indirect bandgap (1.3 eV), MoS_2 also assists in the absorption of incident solar radiation. However, the molybdenum disulfide (MoS_2) layer can also prevent the diffusion of sodium into the absorber layer of CZTS, so accurate control of MoS_2 formation is extremely essential [135]. The absorber layer (p-CZTS/Se, the most important layer) with thickness that ranges from 1 to 2.0 μm is either vacuum or non-vacuum affixed to the Mo back contact. A thin coating of CdS (50–70 nm) (n-type), usually known as the buffer layer, is placed on the absorber layer via CBD to produce a p-n heterojunction with the active layer at the interface, allowing separation of the charge. ZnS, In_2S_3, and several other buffer layers have been investigated apart from CdS. The cell is then finalized by sputtering transparent conducting oxides usually a bilayer of zinc oxide (ZnO). The most widely used zinc oxides are the intrinsic zinc oxide (i-ZnO) and aluminum-doped ZnO (AZO). The cell is usually completed by depositing a metal contact grid usually Ni/Al (Fig. 7), and in some cases, an anti-reflective MgF_2 coating is used so as to capture the incident light more effectively thereby enhancing charge collection and reducing the reflected light loss, which helps to achieve a better performance [53,131,132,136].

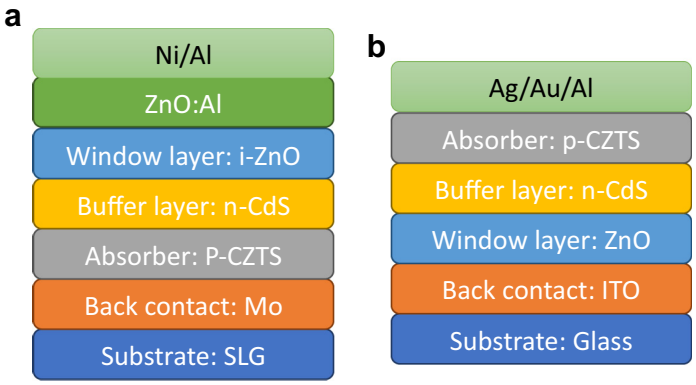

Fig. 7. (a) Substrate architecture and (b) superstrate architecture of a typical CZTS solar cell.

4.1. Working principle of kesterite solar cell

A solar cell is essentially a semiconductor device with p-n junctions. Essentially, all solar cells have the same principle of operation known as the PV effect. The potential difference formed at the junction of two distinct materials in response to visible or other radiation is known as the PV effect. The PV effect as shown in Fig. 8 is characterized by three fundamental processes: charge carriers are generated by absorbing photons in the materials forming the junction, the photogenerated charge carriers are then separated at the junction, and finally, photogenerated charge carriers are assembled at the junction of the terminals. Kesterite solar cell working principle can be comprehended by reference to the band diagram in Fig. 9. The active absorber layer CZTS(Se) is responsible for the electron–hole pairs creation, separation, and movement to the external circuit. Steps 1–4 with red marks show the charge carriers photogeneration and current collection process. In the first and second step, there is an interaction between the incident photon and the CZTS absorber layer, and the photon's energy is moved to an electron in the valence band, leading to the formation of a pair of electron–hole (the electron moves from the valence band to the conduction band forming a hole in the valence band). The first and second steps are known as charge carriers' photogeneration. The PV device must have a p-n junction at the CdS/CZTS(Se) interface to separate the electron–hole pairs formed in the absorber layer of CZTS(Se) (Steps 3 and 4). The integrated space charge region electric field causes the movement of electron and holes in the reverse direction and ultimately reaches the front and back electrodes, respectively. Processes in the third and fourth steps refer to separation of the charge carrier and current collection. The charges that are collected then flows over an external circuit to run an electrical appliance [137–139].

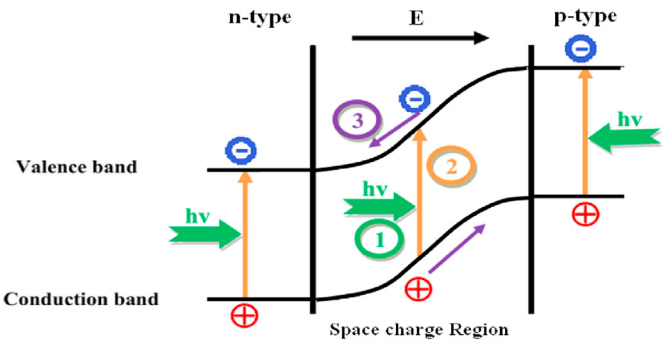

Fig. 8. Mechanism of a p-n junction solar cell. (1) Photon absorption by electrons. (2) Blue-red color indicates the formation of an electron–hole pair. (3) Charge carrier separation induced by an electric field [137].

5. CZTS-superstrate-based solar cells

Unlike the conventional CZTS device architecture that allows any form of substrate to be used, either transparent or opaque, as light passes through the cell before finally reaching the substrate, in superstrate configuration light hits the substrate first before it is absorbed by the solar cell, so the substrate used must be transparent and it is mostly glass (FTO/ITO) and flexible substrates have also been used. Superstrate configuration has an inverse or a reverse configuration of the substrate type configuration. Light is transmitted with the help of a transparent conducting oxide usually indium titanium oxide (ITO) or fluorine doped tin oxide (FTO) and usually coated on a glass substrate preceded by the blocking layer deposition which prevents internal shunting that may arise as the direct contact between p-type semiconductor and the ITO causes large leakage of currents. TiO_2 (compact, dense, tin oxide nanoclusters, nanorods) and ZnO (zinc oxide nanorods) are the two most widely studied window layers for superstrate CZTS, and they are usually deposited by spray pyrolysis, sputtering, doctor blading, or hydrothermal method. After the deposition of the windows layer, a buffer layer is then coated on the window layer so as to enhance the electrical connection between p-type semiconductor (CZTS) and the n-type semiconducting oxide and it also helps avoid photocurrent shunting by preventing electron backflow [140–142]. CdS, ZnS, and In_2S_3 have been reported and deposited by spray pyrolysis, CBD, or nanocrystal layer deposition (NLD) techniques. CZTS is then deposited on the buffer layer by either the vacuum (evaporation, ball milling) or non-vacuum method (molecular precursor solution-spray pyrolysis, sol-gel spin coating, microwave-drop casting, electrodeposition, and precursor solution-spin coating). Finally, the top electrode (carbon paste/graphite, Mo, Ag, or Au) is deposited by either doctor blading or thermal evaporation. Nanostructured CZTS superstrate PVs have the general configuration of glass/metal electrode/metal oxide nanostructure/buffer layer/CZTS absorber/metal electrode [143] and the device architecture for a superstrate CZTS is shown in Fig. 7 (b). Although substrate configuration has shown appreciable efficiency to the tune of 12.6% and almost 13% in laboratory scale devices but the conductivity of the window layer degrades with accelerated aging due to the absorber layer being coarse and the low temperature used for deposition of the layer which influences the interface output between the buffer and the window layer, thereby

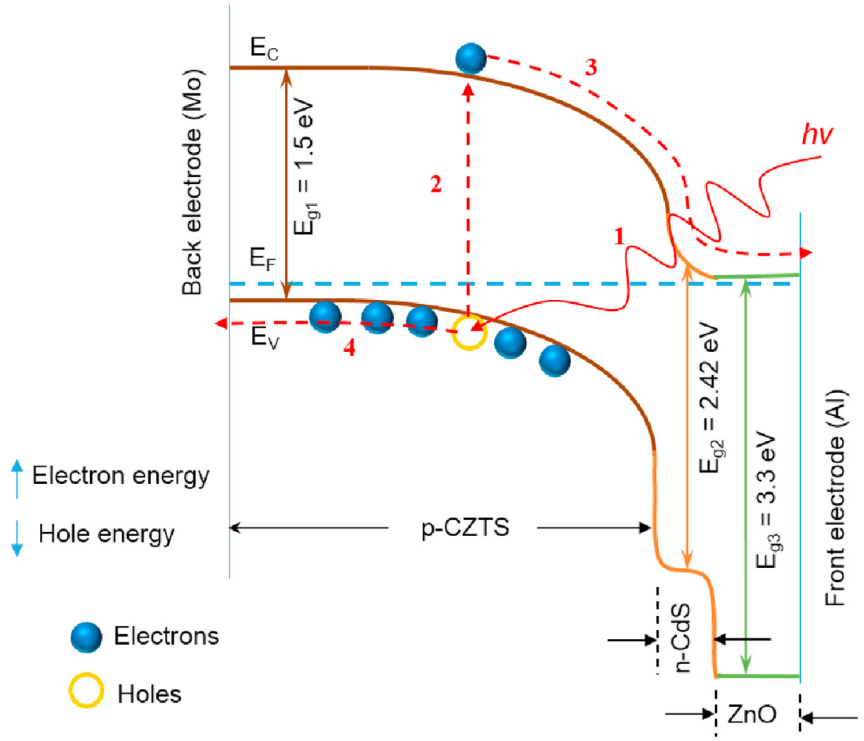

Fig. 9. CZTS-based heterojunction solar cell energy band diagram illustrating band bending at the junction as well as a schematic representation of photogeneration and charge carrier separation [139].

resulting to loss of recombination [129,134]. Superstrate architectural design can be used to overcome the loss of recombination; it offers numerous advantages such as lower cost, facile processes, implementation of light trapping is simple, improvement of the design of the back contact and its implementation in tandem device structures [134]. The next section discusses the few available papers on the method of fabrication of superstrate CZTS solar cells.

6. CZTS-superstrate-based solar cells fabricated by vacuum-based techniques

Vacuum-based method creates a vacuum environment, which enables the uniform deposition of quality films and generates reaction that cannot be achieved under non-vacuum technique. The most used are co-sputtering and evaporation. For superstrate CZTS, only evaporation technique has been found in literature.

6.1. Evaporation technique

Evaporation technique has been a preferred choice for the deposition of CZTS, and it is one of the best techniques for processing highly uniform TFSC [144]. In 2017, S. Varadharajaperumal et al. [145] deposited CZTS thin film via thermal evaporation using a single source prepared from pure elements of the precursors (Cu, Zn, Sn, and S). In this work, the CZTS were thermally deposited on glass/FTO/TiO_2 (1D and 3D)/CdS at 150 °C substrate temperature and annealed at 450 °C, and Au was finally deposited by thermal

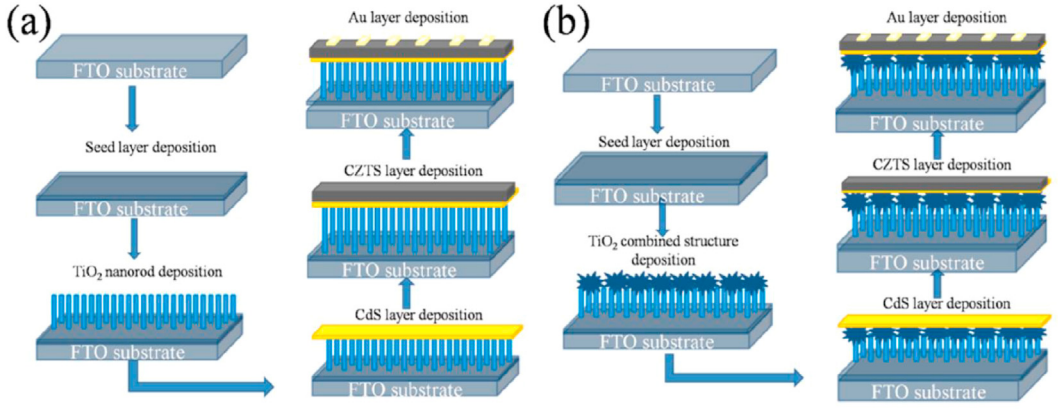

Fig. 10. Photovoltaic device schematics of (a) FTO/TiO_2 nanorods/CdS/CZTS/Au and (b) FTO/TiO_2 mixed structures/CdS/CZTS/Au [Copyright with permission from American Chemical Society] [145].

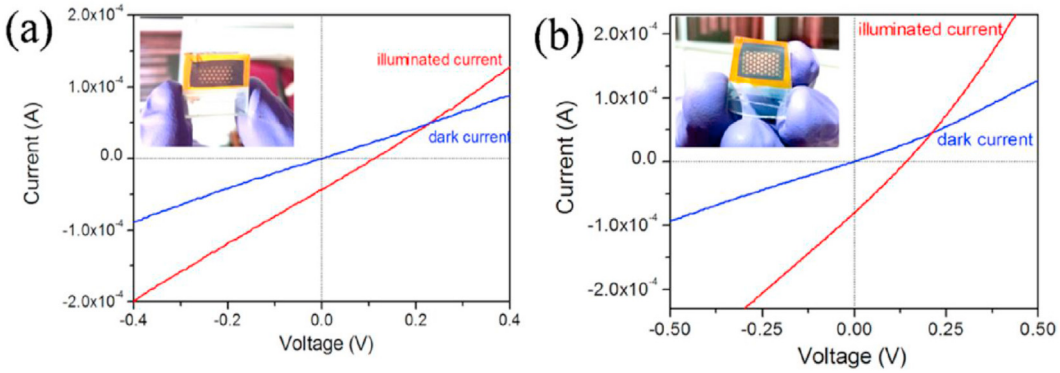

Fig. 11. I–V curves of nanostructured $Cu_2Zn_{1.5}Sn_{1.2}S_{4.4}$/CdS/$TiO_2$ thin film solar cells (a) the nanorods (b) the combined structures. [Copyright with permission from American Chemical Society] [145].

evaporation to complete the device as shown in Fig. 10(a) and (b). Two different devices were made with the TiO_2 nanostructures (combined TiO_2 structures and TiO_2 nanorods). An efficiency of 0.55% was obtained for the device made with TiO_2 nanorods with a V_{OC} of 100 mV, a J_{SC} of 0.042 mA/cm^2, and a fill factor (*FF*) of 23.1%, while the device made with the combined TiO_2 nanostructures exhibited an efficiency of 1.45% with a V_{OC} of 140 mV, a J_{SC} of 0.077 mA/cm^2, and a fill factor of 26.5% with both device having a cell active area of 0.196 mm^2 as shown in Fig. 11(a) and (b). The higher surface area exhibited by the combined nanostructure TiO_2 makes it easier to trap and harvest light compared to TiO_2 nanorods hence a better PCE. The efficiency reported was low because recombination of the electron-hole was fast at the junctions, sulfur was deficient at higher annealing temperatures of greater than 500 °C, and the series resistance experienced by the materials and all these affected the fill factor which then led to reduction in the observed efficiency. Recently, Peksu and Karaagac [146] deposited CZTS thin film by one-step thermal evaporation and fabricated a superstrate device with the configuration SLG/ITO/ZnO-NRs/CdS/CZTS/Ag. The device had an efficiency of 2.82% with a V_{OC} of 460 mV, a J_{SC} of 20.80 mA/cm^2, and a fill factor of 29.5%. The improvement observed in the efficiency as compared to the literature was ascribed to the quality of the CZTS layer, the quality of the interface formed between the core shell components, the morphology, the aspect ratio of ZnO NRs (core), and the chosen material for the metallic top contacts.

6.2. CZTS-superstrate-based solar cells fabricated by non-vacuum-based techniques

Vacuum-based techniques are very expensive and suffer from low-throughput, poor usage of materials and high energy consumption. Profitability is at the heart of every technology so non-vacuum deposition technique is a viable option to achieve solar cell production at low cost [144,147]. Table 1 shows the efficiency achieved for superstrate-based devices by different deposition method including vacuum and non-vacuum based.

6.2.1. Screen printing

It is a less complicated, adaptable, and economically sustainable technology for growing polycrystalline films deposited on large surfaces, and it is ideal for the deposition of other solar cell materials that are based on metal sulfides, selenides, tellurides, and oxides [148]. Qinmiao et al. [149] developed CZTS superstrate solar cell by preparing the CZTS by a combination of ball milling and screen printing method. All the layers were deposited by an entirely non-vacuum method. The windows, buffer, and top electrode were deposited employing spray pyrolysis and screen-printing method, respectively. They studied the annealing duration of screen printed CZTS at 600 °C in nitrogen atmosphere and the influence of buffer thickness on the PCE of the solar cell devices. An increase in the duration of annealing increases the peak intensity and attain maximum when the duration of annealing is 7.5 min, and a decrease in the peak intensity of (112) plane is observed when the duration of annealing was increased further to 10 min. Annealing improves the crystallinity of the CZTS. The annealed samples at 600 °C at different duration had a bandgap ranging from 1.287 to 1.415 eV. The bandgap value improved with an increase in the annealing duration. The best solar cell is that annealed at 5 min and had an efficiency of 0.53%, while the least is the one annealed at 10 min with an efficiency of 0.11%. This efficiency results contradict the XRD results, which shows that the optimal duration of annealing is 7.5 min and this may be ascribed to the thickness of the buffer layer (In_2S_3) as the buffer layer thickness has been mentioned to significantly affect the efficiency of solar cells [150]. The thickness of the buffer layer also had a pronounced effect on the efficiency of the CZTS. The PCE increased from 0.21% to 0.60% when the spray solution increased from 50 mL spray solution to 55 mL spray solution, while it drops to 0.07% when the spray solution was further increased to 60 mL, which is as a result of the highly thick layer prepared under that annealing duration. When a longer annealing duration was used with the 60 mL spray solution, a better thickness was obtained, and the solar cell efficiency increased but the crystallinity decreased. The buffer layer's thickness is very vital for solar cell because it is strongly related to the quality of the p-n junction or the length of carrier diffusion. If the buffer layer is too thin, current leakage may occur, and if it is too thick, the carrier separation rate may be low. The same author using ball milling and doctor blading fabricated a CZTS superstrate solar cell with the configuration glass/FTO/Compact TiO_2/In_2S_3/CZTS/Mo investigating the same parameters as that of the screen-printing method above obtained the highest efficiency of 0.55% [151]. Doctor blade printing technique is a facile, fast, and an economically viable method used for the deposition of thin films on different type of substrates from an ink paste and has the advantage of low material consumption when compared to screen-printing and inkjet printing [152].

6.2.2. Electrodeposition technique

This approach is a very attractive cheap method employed for producing various kind of thin film semiconductor both for pilot scale in research field and large scale for industrial purposes. The technique has been extensively used for CdTe, CIS, and CIGS thin film absorber layer fabrication in solar cell application. There are

Table 1
Device architecture, deposition techniques, and photovoltaic properties of CZTS superstrate-based solar cells.

Device architecture	Deposition methods			Annealing conditions	*Voc* (mV)	*Jsc* (mA/cm^2)	*FF* (%)	PCE (%)	Ref
	Window layer	Buffer layer	Absorber layer						
Glass/FTO/TiO_2NP/In_2S_3/CZTS/ Carbon paste	Compact TiO_2-Spray pyrolysis at 450 °C	In_2S_3-Spray pyrolysis at 200 °C	Ball milling/Screen printing	Dried at 125 °C for 5 min in air and annealed by Rapid Thermal Annealing (RTA) in Nitrogen gas (N_2).	250	8.76	27.0	0.60	[149]
SLG/FTO/Dense TiO_2/TiO_2-nanoclusters/CdS/CZTS/ Graphite electrode	Dense TiO_2-Sputtering TiO_2 nanoclusters-Doctor blading	CdS- Chemical bath deposition at 65 °C	Molecular precursors mixing/Spray pyrolysis at 160 °C	Pre annealed in Nitrogen atmosphere at 140 °C for 30 min, then annealed in Nitrogen atmosphere at 250 °C for 30 min.	564	2.85	43.0	0.51	[153]
Glass/FTO/Compact TiO_2/In_2S_3/ CZTS/Mo	Compact TiO_2-Spray pyrolysis at 450 °C	In_2S_3-Spray pyrolysis at 200 °C	Ball milling/Doctor blading	Annealed by Rapid Thermal Annealing (RTA) process in N_2 at 400 and 500 °C for 5 min and at 600 °C for 1–11 min.	240	7.82	29.0	0.55	[151]
SLG/FTO/Dense TiO_2/TiO_2-nanoclusters/CdS/CZTS/ Graphite electrode	Dense TiO_2-Sputtering TiO_2 nanoclusters-Doctor blading	CdS- Chemical bath deposition at 65 °C followed by annealing at 250 °C	Molecular precursors mixing/Spray pyrolysis at 160 °C	Pre annealed in Nitrogen atmosphere at 140 °C for 30 min, then annealed in Nitrogen atmosphere at 300 °C for 30 min.	445.9	6.794	37.4	1.131	[154]
SLG/ITO/ZnO NRs/CdS/CZTS/Au	ZnO NRs- Spin coating of sol gel ZnO seed layer preceded by hydrothermal growth of ZnO NRs	CdS- Nanocrystal layer deposition for 50 min	Precursor solution/Spin coating	Annealing done in air at 150 °C for 10 min followed by at 250 °C for 10 min.	679.2	4.1	43.8	1.200	[143]
Glass/ITO/ZnO NRs/ZnS/CZTS/ Au	ZnO NRs- Hydrothermal growth on spin coated sol gel ZnO seed layer	ZnS-Chemical bath deposition at 70–80 °C for 6 –24 h	Sol-gel/Spin coating	Preheated at 150 °C for 10 min on a hotplate in air followed by at 250 °C for 10 min.	868.9	8.50	49.1	3.63	[52]
Glass/FTO/TiO_2/In_2S_3/CZTS/ Graphite	TiO_2- Spray pyrolysis	In_2S_3-Spray pyrolysis	Electrodeposition	Annealed in sulfur atmosphere at 580 °C for 90 min.	615.0	13.9	41.0	3.53	[155]
Flexible substrate/FTO/ZnO NRs/CZTS/Carbon conductive adhesive tapes	ZnO NRs- Hydrothermal growth on ZnO seed layer deposited by RF sputtering.	N/A	Microwave/Drop casting	N/A	405	4.35	46.9	0.83	[156]
Glass/FTO/TiO_2 NRs/CdS/CZTS/ Au	TiO_2 NRs- Hydrothermal growth on TiO2 seed layer deposited by DC magnetron sputtering	CdS-Chemical bath deposition at around 70 °C for 3–4 min.	Thermal evaporation	Annealed at 450 °C for 15 min	100	0.042	23.1	0.55	[145]
Glass/FTO/Dense-TiO_2/CdS/ CZTS/Au	Dense TiO_2-Spray pyrolysis	CdS-Chemical bath deposition	Precursor solution deposition/Spray pyrolysis	Annealed in N_2 atmosphere	474.0	5.07	44.0	1.05	[157]
Glass/FTO/ZnO NRs/ZnS/CZTS/ Au	ZnO NRs- Hydrothermal growth on ZnO seed layer deposited by spin coating	ZnS-Chemical bath deposition at 60 °C.	Sol-gel/Spin coating	Pre annealed at 120 °C for 10 min and subsequently at 300 °C for 1 h in a furnace.	454.0	5.652	41.6	1.07	[158]
Glass/FTO/ZnO NRs/ZnS/CZTS/ Au	√	√	√	√	285.0	0.837	35.9	0.08	
Glass/FTO/TiO_2/CdS/CZTS/Au	TiO_2 NRs- Hydrothermal growth	CdS-Chemical bath deposition at 65 °C for 11 min.	Molecular precursor solution/Spin coating	Annealed in a tubular furnace at 250 °C for 1 h in Ar atmosphere.	518	5.143	–	1.04	[134]
SLG/FTO/ZnO NWs/CdS/CZTS/ Ag	ZnO NWs-Hydrothermal on ZnO seed layer deposited by spin coating.	CdS-Nanocrystal layer deposition for 20–70 min at room temperature	Precursor solution deposition/Spin coating	Preheated on a hotplate at 200 °C for 2 min followed by at 250 °C for 40 min.	589	7.07	54.0	2.27	[159]
Glass/FTO/CdS/CZTS/Ag	–	CdS- SILAR	SILAR	Dried on a hotplate at 50 °C	733	7.494	45.0	2.475	[160]
Glass/FTO/Compact TiO_2/CdS/ CZTS	Compact TiO_2	CDS-Chemical bath deposition at 65 °C for 15 min.	SILAR	Annealed at 200 °C for an hour.	–	–	–	–	[161]
SLG/ITO/ZnO-NR/CdS/CZTS/Ag	ZnO NRs-Hydrothermal growth on ZnO seed layer deposited by sputtering	CdS- Chemical bath deposition	CZTS- One-step thermal evaporation	400 for 30 min under the flow of N2	460	20.8	29.5	2.82	[146]

two dissimilar approaches for preparing CZTS thin films: sequential electroplating or one-step electrodeposition of the precursors preceded by reactive annealing in a sulfur or selenium atmosphere [103]. Depositing quaternary system such as CZTS or CZTSSe by one-step electrodeposition is more complicated compared to binary system such as CdTe. A better way to simplify it is by depositing the metal precursor layers as a stack in stoichiometric amount, then reactive annealing in a sulfur or selenide atmosphere in order to transform the metal multilayer to CZTS or CZTSSe. Another way is to simultaneously deposit the three metals so as to create an intimate mixture of the elements and subsequently transformed to CZTS or CZTSSe by sulfurization or selenization. In both cases, if the chalcogenide precursor is not present, the electrochemistry only favors the reduction of the metal ions [162]. An entirely non-vacuum method of deposition of all the layers was reported by Berruet et al. [155]. In their method, the buffer and windows layer were coated by spray pyrolysis, CZTS absorber layer was deposited via electrodeposition, while the conductive graphite ink acting as the back contact was deposited by painting using a mask to define the areas. The CZTS superstrate solar cell fabricated showed an improvement in the PV properties as compared to previous report with TiO_2 and In_2S_3 as n-type semiconductor [149,153]. An efficiency of 3.53%, a V_{OC} of 0.615 V, a J_{SC} of 13.9 mA/cm^2, and *FF* of 0.41 was obtained, which is among the highest known efficiency reported for a CZTS superstrate solar cell.

6.2.3. Successive ionic layer adsorption and reaction (SILAR) technique

SILAR is an advanced CBD method, and it is similar to atomic layer deposition method for depositing thin films [163]. SILAR was first performed by Ristov et al. in the year 1985 [164] and the name SILAR was given by Nicolau and his colleagues in the same year [165]. SILAR unlike CBD avoids heavy precipitate formation [166] and aside from being a very simple deposition technique, it can be employed for thin film deposition without the use of an expensive technology, the maintenance requires no expensive equipment, requires no quality substrates or target, relatively inexpensive, no high heating required, making it economically feasible for large scale deposition of thin film solar cells. It can be performed using simple laboratory equipment such as beaker [167]. The basic steps involve dipping the substrate into the cationic solution and then rinsing with deionized water to eliminate loosely bound cations and subsequently dipped into the anionic solution and then rinsed with deionized water to eliminate unreacted anions from the substrate. The dipping was performed several times in cationic and anionic solution in order to achieve the desirable thickness. It is necessary to rinse with deionized water after each dipping step so as to allow for thin film formation on the substrate and also to avoid precipitate formation in the solution [163,166,167]. Jasmitha et al. [160] fabricated a CZTS superstrate solar cell without a windows layer. CdS and CZTS absorber layer were deposited by SILAR method. CdS was deposited by immersing the substrate in a methanolic solution of cadmium acetate for 2 min; it is then rinsed with methanol and deionized water, then dried at 60 °C. The substrate is then immersed in the methanolic solution of sodium sulfate for 2 min and subsequently rinsed with methanol and deionized water and then finally dried. The immersion and drying method were repeated seven times to realize the desired thickness. CZTS was deposited by immersing the glass/FTO/CdS substrate in a solution of the metal chlorides (cationic solution) for 30 s and then washed with deionized water followed by drying at 50 °C and followed by immersion in an anionic solution of sodium sulfate for 30 s and then dried at 50 °C on a hotplate. The immersion and deposition cycles were repeated for 30 times to the desired thickness of CZTS on glass/FTO/CdS. XRD analysis confirmed the tetragonal phase of the kesterite crystal structure having a crystallite size of 35 nm with a 1.3 eV bandgap. EDS results also confirm an almost stoichiometric ratio of 2:1:1:4 for CZTS. An efficiency of 2.475%, a V_{OC} of 0.733 V, a J_{SC} of 7.494 mA/cm^2, and *FF* of 0.45 was obtained for the fabricated CZTS superstrate solar cell. Krishnan et al. [161] explored the electrical properties of a CZTS superstrate P–N junction with the configuration glass/FTO/Compact TiO_2/CdS/CZTS without fabricating a solar cell. All the layers were deposited by solution-based method. The P–N junction had a resistivity of approximately 1.51×10^2 Ω cm, a carrier concentration of 1.28×10^{17} cm^{-3}, and a mobility of 0.32 cm^2/V/s. The limited mobility is caused by the thin film's small grain size, which caused electron and hole recombination at the grain boundaries. A knee voltage of close to 1 V was obtained for the P–N junction, indicating that an excellent V_{oc} can be projected from solar cell fabricated with glass/FTO/TiO_2/CdS/CZTS.

6.2.4. Sol-gel-based spin coating technique

It is a facile, cost-effective process for producing many types of semiconductor thin films [103]. Among the chemical deposition techniques, the spin-coating technique has numerous advantages such as it is easy to handle, the elemental constituents can be mixed in a precursor colloidal solution at a molecular level. Sol-gel consists of nanoparticles polycondensation, and thus, thin films with improved crystallinity can be gotten at a lower annealing temperature and transfer of a consistent composition from gel to thin films due to deposition at room temperature [168]. Three steps are usually involved when fabricating a thin film by spin coating method: first, the precursor solution containing the specific ion is prepared; second, the precursor solution is spin coated on a glass substrate to create the film, and lastly, the thin films is annealed in a particular atmosphere [169]. This method was first introduced for the production of CZTS thin films by Tanaka et al. in 2007 [170]. In 2016, Ghosh et al. [52] were the first to report on the substitution of CdS with ZnS for a CZTS superstrate solar cells grown on a vertically aligned ZnO nanorods arrays. In this work, ZnO nanorod arrays that aligned vertically was grown by first spin coating the seed layer of ZnO synthesized by mixing zinc acetate dihydrate (precursor salts), 2-methoxyethanol (solvent), and monoethanolamine (stabilizer) at 60 °C for 2 h, and subsequently, the ZnO nanorods were grown by placing the seed layer-coated substrate upside-down in a beaker at 90 °C for 5 h (hydrothermal method). ZnS layer was coated on the ZnO nanorods by CBD by incubation in an aqueous sodium sulfide solution at 70–80 °C for 6–24 h to obtain the ZnS-coated ZnO nanowires. Then, CZTS was deposited on the ZnS-coated ZnO nanowires by sol-gel spin coating method, and finally, a 100 nm thin film of gold metal was coated to complete the solar cell. Fig. 12(a) and (b) shows the block diagram and the energy band diagram of the fabricated CZTS superstrate solar cell, respectively. ZnO nanorods serve as the electron-transport layer since its work function matches that of the acceptor and they also exhibit high electron mobility. ZnS was chosen because it is environmentally friendly, non-toxic, and relatively cheap, and its main function is to enhance the alignment of the energy band between CZTS acceptor and the ZnO window layer; it reduces the density of the surface defect at the interface as well as increases the charge carrier's lifetime. The fabricated device as shown in Fig. 12(c) and (d) had *FF* of 0.491, a V_{OC} of 868.9 mV, a J_{SC} of 8.50 mA/cm^2, and an efficiency of 3.63%, which is currently the champion of the CZTS superstrate based solar cell. The improvement observed in the V_{OC} was attributed to a better electron affinity and ionization potential when compared to CdS, while the small improvement observed in the fill factor is as a result of an improved transport and collection of

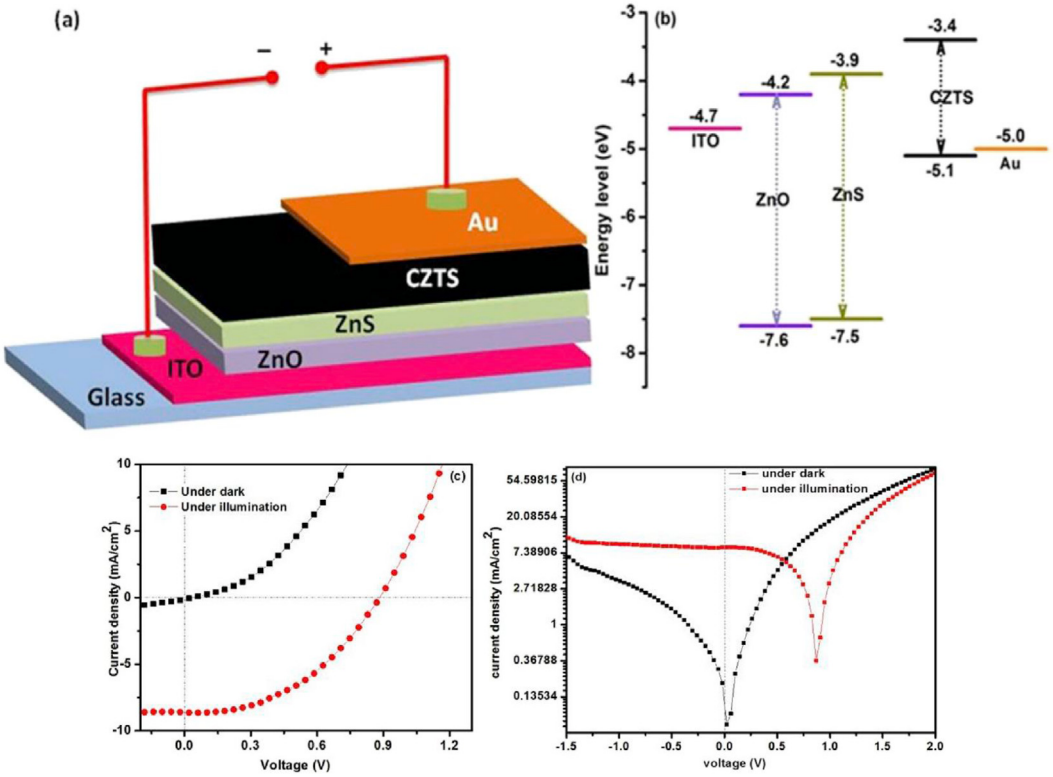

Fig. 12. ITO/ZnO/ZnS/CZTS/Au solar cell (a) block schematic (b) energy diagram (c) I–V characteristics of the entire solar cell under illumination, and (d) semi-log of I–V [Copyright with permission from Elsevier] [52].

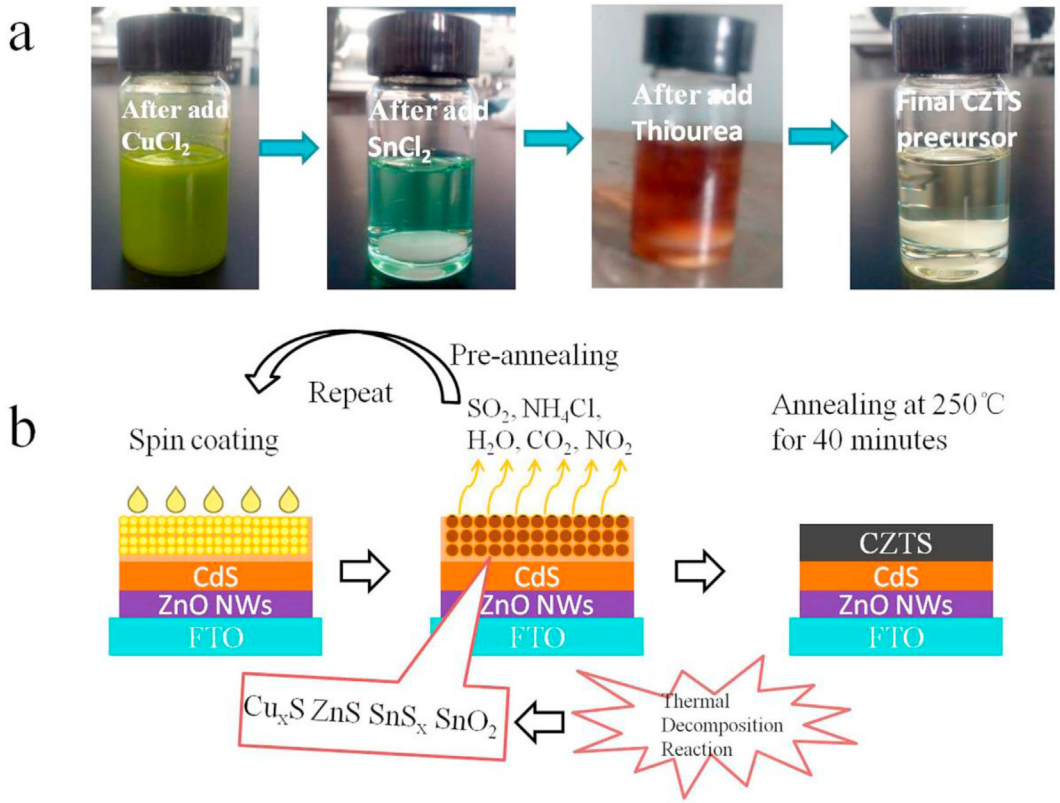

Fig. 13. (a) A visual representation of each step precursor solutions for the CZTS preparation. (b) An illustration of how CZTS thin films is formed via the sol-gel route by thermal decomposition reaction [159].

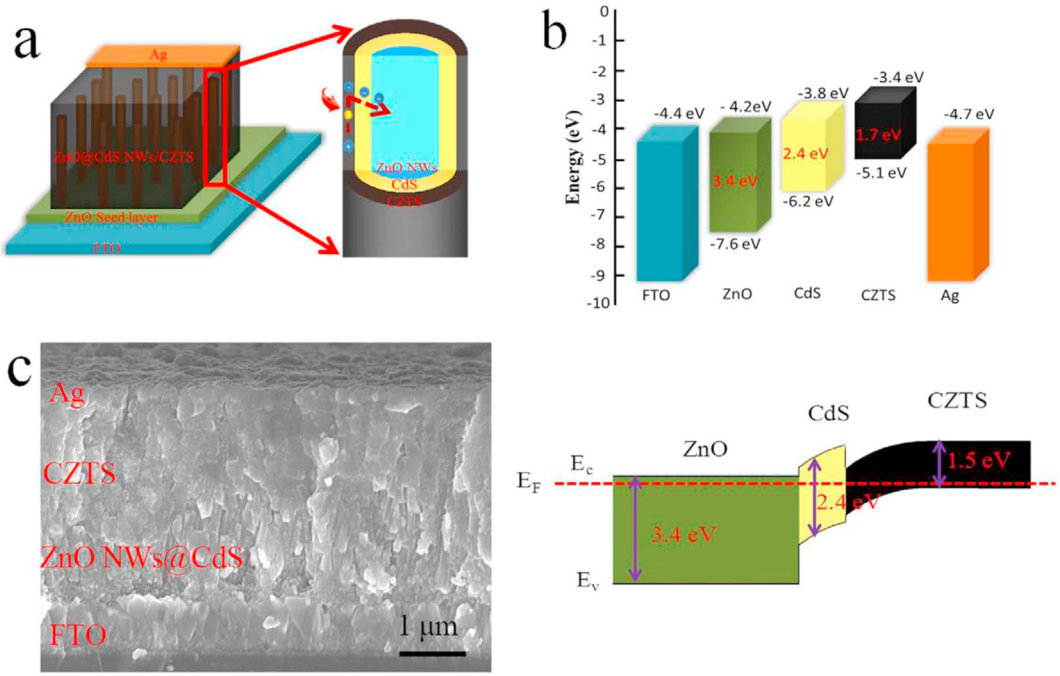

Fig. 14. (a) A ZnO@CdS NWs-based inverted-structure CZTS solar cell (FTO/ZnO@CdS NWs/CZTS/Ag). (b) The alignment of the bandgap of each layer in a CZTS solar cell. (c) SEM image of the completed device (FTO/ZnO@CdS NWs/CZTS/Ag) in cross section [159].

charges owing to the integration of a ZnO nanorod arrays that are vertically aligned.

In the same year, Chen et al. [159] developed ZnO@CdS nano heterojunction arrays with low dimensions as window and buffer layer in a CZTS superstrate solar cell. A 2 μm in length and approximately 50–60 nm hexagonal arrays of ZnO nanowires were obtained by hydrothermal synthetic method at 90 °C for 30–90 min. Prior to the growth of the ZnO nanowires, a ZnO seed layer prepared by mixing zinc acetate dihydrate, diethanolamine in dimethylcarbinol at 50 °C for 1 hr was spin coated on the FTO substrate. The CdS was deposited on the ZnO nanowires by NLD techniques at room temperature for 20–70 min. CZTS absorber layer was then coated by sol-gel spin coating method as shown in Fig. 13(a) and (b). The cell was then completed by deposition of Ag. They showed that the morphology of ZnO nanowires, buffer layer, thickness of CdS and CZTS crystallization temperature had pronounced effect on the PV efficiencies of the fabricated CZTS superstrate devices. Fig. 14(a)–(c) shows the fabricated inverted structure, the band alignment, and the cross-sectional SEM image of FTO/ZnO@CdS NWs/Ag. When the device was fabricated without any buffer layer and with the configuration FTO/ZnO NWs/CZTS/Ag, the device exhibited low PV efficiency since it has been shown that the buffer layer enhances the efficiency of CZTS solar cells by preventing unwanted shunt paths and expanding the depletion distance at the p-n interface, which extends the electrical field in the absorber layer thereby minimizing the loss of collection by tunneling and recombination [171].

The PV performance was enhanced when it was coated with CdS, and different thicknesses were obtained as a function of the deposition time. An increase was first observed in the PV efficiency as the CdS thickness increases and then decreases with a further increase in efficiency, and the best thickness that yielded a higher PCE was observed when CdS was deposited for 50 min. The ZnO nanowires with a length of 2 μm and CZTS device annealed at 250 °C gave the best efficiency of 2.27%, a V_{OC} of 0.589 V, a J_{SC} of 7.07 mA/cm^2, and *FF* of 0.54. ZnO nanowires allow for the loading of more CZTS nanoparticles, leading to an enhancement in photo absorption and the one-dimensional ZnO arrays enables excellent charge carrier transport to be matched with broad interface areas for the charge separation and transport with the neighboring species.

Recently, the effect of shunt and series resistance on the performance of ZnO nanowire based CZTS superstrate solar cell was investigated by Gayen and Chakrabarti [158] using sol-gel spin coating technique for the deposition of CZTS. They fabricated the cell with the configuration FTO/ZnONW/ZnS/CZTS/Au. The window layer which is the ZnO nanowires was grown by first spin coating a seed layer of zinc oxide prepared from a solution of zinc acetate dihydrate and ethanolamine dissolved in isopropanol at 60 °C for 1 h followed by the growth of the ZnO nanowires by hydrothermal method. ZnS layer was coated on the windows layer by CBD to obtain the ZnS-coated ZnO nanowires. Then CZTS was deposited on the ZnS-coated ZnO nanowires by sol-gel spin coating method and finally a gold metal contact was deposited by e-beam evaporation technique to complete the solar cell. It was observed that the series (R_s) and shunt resistances had a pronounced impact on the parameters of the fabricated heterojunction solar cells. A large R_s value leads to a reduction in the short circuit current (J_{sc}) while a small R_{sh} value reduces the open circuit voltage (V_{oc}) and on combining both effects, the fill factor reduces drastically thereby reducing the performance of the cell. The cell fabricated with ZnS exhibited a PCE of 1.07%, a V_{OC} of 0.454 V, a J_{SC} of 5.652 mA/cm^2 and *FF* of 0.416 while the cell without ZnS show a poor PV characteristic with a PCE of 0.08%, a V_{OC} of 0.285 V, a J_{SC} of 0.837 mA/cm^2 and *FF* of 0.359. This shows that the large interface defects were passivated by ZnS buffer layer which as a result lead to the reduction in the series and shunt resistances thereby leading to an increase in the current which then therefore leads to a better PV efficiency.

6.2.5. Molecular precursor solution

It is one of the most easy and efficient ways for processing films of multinary compound system and the elemental component can

be independently adjusted to regulate the composition and phase of the compound [172]. It usually involves dissolving the metal compounds such as metal salts, sulfides or metals in a particular solvent to form a homogenous solution with capabilities to yield chemically clean films [172,173]. Lee and Yong in 2013 [143] prepared molecular salts from copper iodide, zinc acetate, tin chloride and thioacetamide in pyridine. The precursor salts were added one after the other in order to prevent the formation of an undesired precipitate. To compensate for the loss of sulfur excess thiourea was used. The cell had a configuration of ITO/ZnO NRs/CdS/CZTS/Au. The ZnO nanorods were grown by hydrothermal technique on the SLG ITO substrate. CdS was deposited on the ZnO nanorods substrate by NLD by incubating the ZnO nanorod substrate in a solution of cadmium chloride and thioacetamide for 50 min. CZTS was spin coated on the SLG/ITO/ZnO NR/CdS from the prepared molecular precursor solution and dried at 150 °C and immediately transferred to a hotplate already preheated to 250 °C. The device was completed by depositing gold as the top electrode. The cell had an efficiency of 1.2%, a V_{OC} of 679.2 mV, a J_{SC} of 4.1 mA/cm^2, and *FF* of 0.438.

More recently, Satale and Bhat [134] studied the effect of different atomic ratios on CZTS superstrate solar cell. The fabricated PV device had an architecture of glass/FTO/TNR/CdS/CZTS/Au. The TiO_2 nanorods (TNRs) was synthesized by placing a pre-cleaned FTO substrates in a 50 mL Teflon autoclave containing a nutrient solution of $TiCl_4$ dissolved in a mixture of concentrated HCl and deionized water. The autoclave was placed in an electric oven at 180 °C for 2 h. Upon the conclusion of the reaction, the substrate was removed and washed thrice with distilled water and annealed in air for an hour at 450 °C 60 nm of CdS buffer layer was coated on the TiO_2 nanorods by CBD at 65 °C for 11 min before drying in an electric oven at 120 °C for 5 min. The CZTS absorber layer was spin coated on the CdS-coated substrate from the two prepared molecular precursor solution. The coating was done a few times to obtain a homogeneous film of the required thickness. Afterward, the substrates coated with CZTS were annealed in a tubular furnace under argon atmosphere for 1 h at 250 °C. Thermal evaporation was used to deposit a 100 nm gold metal to finalize the device. FESEM image revealed that sample CZTS2 had a smooth film surface with no noticeable pin holes or cracks, while sample CZTS1 had a non-uniform surface with cracks. Sample CZTS1 and CZTS2 exhibited a bandgap of 1.57 and 1.42 eV, respectively. The PV properties are shown in Fig. 15. The device fabricated with sample CZTS1 had a V_{OC} of 0.507 V, a J_{sc} of 4.144 mA/cm^2, while sample CZTS2 had a V_{OC} of 0.518 V, a J_{SC} of 5.143 mA/cm^2, and an efficiency of 1.04%. The efficiency and short circuit current of sample CZTS2 were approximately 16.67% and 20.46% higher than that of sample CZTS1. The better efficiency and an increase in the current density observed for sample CZTS2 can be ascribed to the improved crystallinity, optimum composition, purer phase formation, uniform and crack-free films, and longer carrier diffusion length as shown by the FESEM, XRD, Raman, and EDS analyses.

6.2.6. Spray pyrolysis deposition

This technology has been extensively employed for the production of thin films. The method is simple, easy to handle, the engineering design is less complex, and the technique offers good reproducibility which is advantageous for producing any kind of thin films on a large scale. No vacuum is required for its deposition making it suitable for large scale industrial applications [103,174]. Nakyama et al. [175] were the first to synthesize CZTS by spray pyrolysis deposition technique while Kurokawa and Ito [153] were the first to report superstrate CZTS solar cell fabricated by spray pyrolysis deposition technique. They fabricated a device with the configuration SLG/FTO/TiO_2/CdS/CZTS/graphite electrode. The

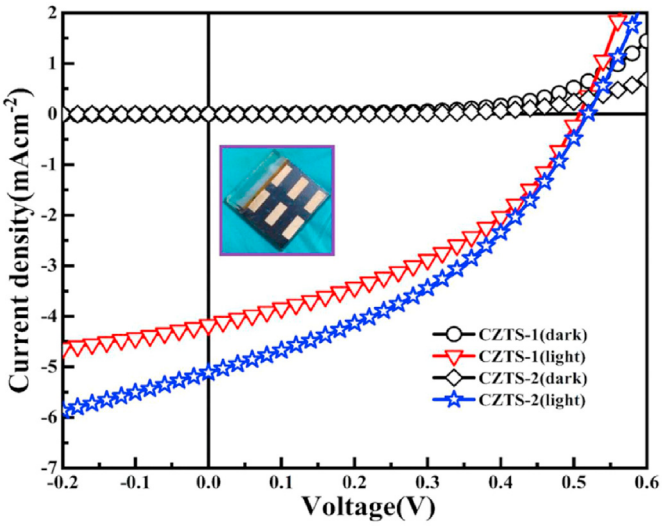

Fig. 15. J-V curves of the superstrate (CZTS) solar cell devices constructed with CZTS-1 and CZTS-2 molecular precursors. The digital image of the actual device is shown as inset. [Copyright with permission from Elsevier] [134].

nanocluster TiO_2 and dense TiO_2 were deposited by doctor blading and sputtering technique, respectively. CdS layer was coated on the TiO_2 by CBD process varying the time of deposition from 5 to 30 min. CZTS was then coated on the TiO_2 by spray pyrolysis deposition method from solution made by mixing copper acetate monohydrate, tin chloride dihydrate, zinc acetate dihydrate, and sulfur powder in dimethylformamide and monoethanolamine as solvent and stabilizer. The solution was sprayed at 160 °C before drying in air for 5 min and the procedure was repeated for five times followed by pre-annealing at 140 °C for 30 min and finally dried at 250 °C for 30 min. The cell was completed by forming graphite electrode on the CZTS absorber. They showed that CdS layer thickness did not change with respect to time but had a considerable impact on the PV properties of the solar device. An efficiency of 0.51% was obtained when CdS was deposited at 20 min with a J_{SC} of 2.85 mA/cm^2, a V_{OC} of 0.564 V, and *FF* of 0.43. The reason for the low performance was because the cell suffered from large series resistance, thereby leading to a reduction in the *FF*, J_{SC}, and the PCE. Using the same configuration, same procedure and same deposition technique as above except for annealing at 250 °C after CdS deposition and final annealing carried out at 300 °C, Kunihiko et al. [154] reported an efficiency of 1.131%, a V_{OC} of 0.4459 V, a J_{SC} of 6.794 mA/cm^2, and *FF* of 0.374. The reason for the increase in efficiency as compared to the previous one maybe because the holes in the CZTS/nc-TiO_2 surface were reduced thereby leading to a reduction in current leakage and consequently leading to a higher J_{SC}.

Recently, Zhong et al. [157] employed the process of spray pyrolysis to deposit CZTS from the solution made by combining zinc chloride ($ZnCl_2$), tin chloride ($SnCl_2$), copper chloride ($CuCl_2$), and thiourea in methanol. The FTO substrate used was first cleaned and a dense layer of TiO_2 was deposited by spray pyrolysis followed by the coating of CdS (50 nm) by CBD. The CZTS was deposited on the CdS-coated TiO_2 substrate by spray deposition at 350 °C and subsequently annealed under nitrogen atmosphere. XRD and Raman analyses confirmed that pure kesterite phase was formed. The bandgap was found to be 1.72 eV, which is way above what is usually reported in the literature, and the reason is because the film prepared by spray pyrolysis was thin, but the film thickness is still consistent with superstrate-type CZTS solar cell absorber. The

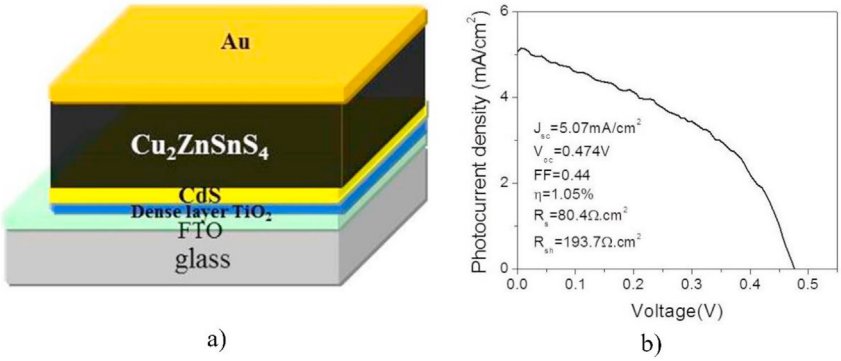

Fig. 16. (a) FTO/d-TiO_2/CdS/CZTS/Au superstrate solar cell schematic (d-TiO_2, as the hole-blocking layer). (b) J-V properties of FTO/d-TiO_2/CdS/CZTS/Au solar cells illuminated with AM 1.5G. (100 mW/cm^2) [157].

fabricated superstrate CZTS solar cell (Fig. 16) had a configuration of glass/FTO/d-TiO_2/CdS/CZTS/Au with an efficiency of 1.05%, a V_{OC} of 474 mV, a J_{SC} of 5.07 mA/cm^2, and *FF* of 0.44. The cell had a low efficiency because of low shunt resistance and large series resistance caused by the poor quality of the crystals and the severe recombination. Another reason was because of the too thin CZTS absorber layer which was not sufficient enough to absorb enough light that can sufficiently produce light-induced charges thereby resulting in the generation of a low photocurrent. Another way suggested to increase the efficiency of the device is by annealing in the presence of sulfur or H_2S atmosphere as this makes the thin film denser thereby improving the quality of the crystals, which invariably improves the efficiency of the solar cell device.

6.2.7. *Microwave technique*

In the electromagnetic spectrum, microwave falls in between radio and infrared waves and are electromagnetic waves with a frequency of 0.3 GHz−300 GHz (wavelengths varying from 1 mm to 1 m). Both microwave ovens for kitchen and the bulk of microwave reactors available commercially for chemical synthesis run at a wavelength of 12.24 cm, which corresponds to a frequency of 2.5 GHz [46,47]. Microwave chemistry is the science of employing microwave irradiation to accelerate chemical processes, and it is based on efficiently heating materials by microwave dielectric heating not initiating chemical reactions through direct absorption of electromagnetic energy, as in photochemical processes (i.e., the ability to absorb and transform microwave energy into heat from a particular material (e.g., solvents and or reagents) [176]. The mechanism of microwave heating involves two key processes, that is, dipolar polarization and ion conduction [46]. Unlike traditional laboratory heating methods that typically require using an electric furnace/an oil bath to heat the reactor walls, then heats the reactant by convention or by conduction with the reactor acting as an intermediary for transferring heat energy via an external heat source until it gets to the solvent, then eventually to the reactants, which takes longer to reach the desired temperature thereby leading to temperature differences in the bulk medium, non-uniform, and an ineffective reaction, which could result in serious problems in large-scale production, microwave heating instead heats the target materials directly without heating the whole furnace/oil bath minimizing energy and time resulting in comparatively cost effective, energy-efficient, and high material production efficiency [176]. For the above reasons, microwave synthetic method has received tremendous attention in the field of nanomaterials. For the synthesis of CZTS nanomaterials, it generally involves dissolving the cationic and anionic source in a high microwave absorbing solvent, which is then placed in a laboratory microwave reactor or a kitchen microwave at particular reaction conditions such as microwave power, temperature, and time. The product obtained is then centrifuged, washed severally with

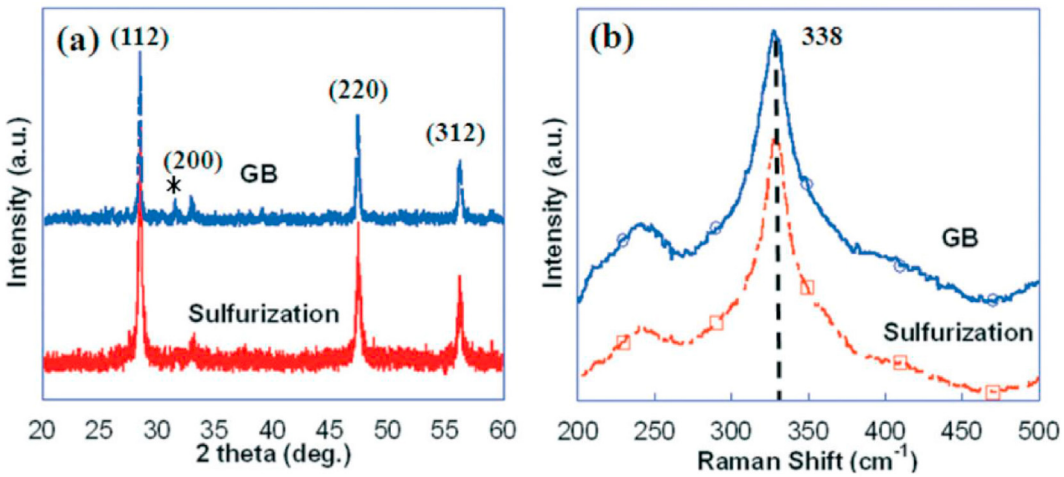

Fig. 17. (a) XRD pattern of the annealed CZTS in the glove box (GB) and sulfurized CZTS (b) Raman spectrum of the annealed CZTS in the glove box (GB) and sulfurized CZTS. [Copyright with permission from Royal Society of Chemistry] [180].

solvents, and then dried at a particular temperature for a particular time [41,177–179].

Colloidal CZTS nanoparticle inks were first synthesized using microwave assisted method by Flynn et al. [110]. Metal chloride salts of Cu, Zn, and Sn was utilized as the cationic source, while thioacetamide was the source of sulfur and were dissolved in ethylene glycol in one pot targeting an initial precursor concentration with nanoparticle composition of copper poor and zinc rich. The use of metal chlorides ensures that all the species had the same counter ions and better chemical uniformity in solution at 190 °C for 30 min. Their findings show that varying the initial precursor concentration could be used to control the composition of the nanoparticles and that reactions carried out with excess zinc and a decrease in copper were required to achieve ideal values of 0.86 for Cu/(Zn + Sn) and 1.04 for Zn/Sn. XRD and Raman pattern confirmed the synthesis of high-quality CZTS kesterite crystal phase.

Wang and co-workers [180] developed Cu_2ZnSnS_4 (CZTS) nanoparticles via one pot facile microwave-assisted heating employing metal acetylacetonates, sulfur and oleylamine as cationic precursor salts, anionic precursor salt, and solvent, respectively. Annealing of the materials was carried out at two dissimilar environments, one in low oxygen and H_2O at less than 0.5 ppm in the glove box (GB), whereas the other was done in an atmosphere of sulfur designated as sulfurization, at 500 °C for 30 min. The XRD pattern and Raman spectra (Fig. 17) revealed that the CZTS annealed in the GB contains an impure phase compared to the sulfurized annealed sample and the probable reason proposed for the presence of the impure phase was because it lacks sulfur, which led to the presence of other phases of chalcogenide compounds. This is consistent with many reports in the literature indicating that an anion is lost during the process of CZTS annealing. CZTS thus appears to have secondary phases such as CuS, Sn_2S_3, and SnS_2 when annealed without sulfur while CZTS annealed in the GB have secondary compounds coming from CuS and Sn_2S_3. The bandgaps were estimated to be about 1.46 and 1.5 eV for CZTS annealed in the GB and an atmosphere of sulfur, making them suitable for PV applications.

CZTS nanopowder was synthesized in aqueous media by varying the reaction time and thiourea concentration [181]. An ammonium hydroxide mixture was added to facilitate in the production of water-soluble metal amine complexes, thus preventing unwarranted and rapid metal sulfides precipitation, and keeping significant number of metals in the solution. XRD results revealed that several undesirable peaks unrelated to CZTS phase were detected when the reaction was carried out with the appropriate concentration of thiourea to form Cu_2ZnSnS_4, and it was observed that the CZTS phase improved as thiourea concentration increases. Two important things were observed as the concentration of thiourea increases. First, the individual metal sulfide peaks continue to disappear, and second, when compared to distinct metal sulfide peaks, CZTS relative intensity increased. They established that a higher concentration of thiourea was optimal to attain a superior CZTS phase even though CZTS mechanism of formation as a function of concentration of thiourea was not fully understood. They found out that the higher the time, the better the purity. Raman and EDAX also established the formation of CZTS. The particle size ranges from 150 to 600 nm. Scanning electron microscopy (SEM) image showed the nanopowder was of irregular shape, and transmission electron microscopy (TEM) analysis confirmed a flower-like resembling morphology for 2D CZTS layer structures. The optical absorption spectra of CZTS nanopowder exhibited strong absorbance in the solar spectrum visible region with a calculated bandgap of 1.27 eV, suggesting its potential as a relatively good absorber layer for thin film PV cells [182].

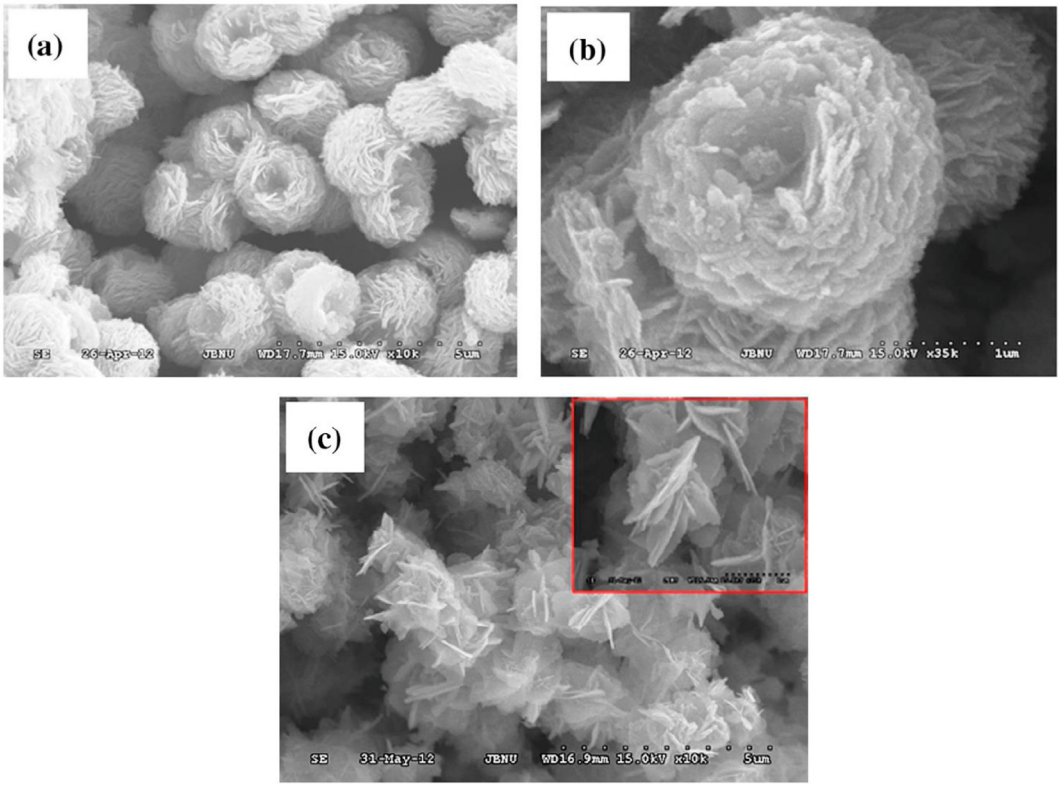

Fig. 18. : (a) A low and (b) high resolution SEM images of CZTS particles synthesized with PVP addition and (c) without PVP addition [Copyright with permission from Elsevier] [183].

Kumar et al. [183] described the first synthesis of microwave-assisted of doughnut-shaped Cu_2ZnSnS_4 (CZTS) hierarchical microparticles utilizing N,N-dimethylformamide (DMF) as a solvent and polyvinylpyrrolidone (PVP) as a stabilizer, respectively. They examined the effect of polyvinylpyrrolidone effect on the formation of CZTS nanoparticles. XRD and Raman analyses established that a single pure kesterite (CZTS) phase was formed. SEM image with low magnification (Fig. 18) showed that the CZTS particles with PVP consisted of nearly homogeneous CZTS microparticles with doughnut-like shape ranging in size from 1 to 2 μm and that those synthesized without PVP shows several plate-like-shaped particles of about 50–60 nm thickness. The plate-like-shaped particles are distributed at random to form aggregates of various sizes and shapes. Therefore, SEM image revealed that polyvinylpyrrolidone played a vital role in forming a hierarchical doughnut-shaped architecture. PVP has successfully been used as a stabilizer and a structural-directing agent to prepare numerous new well-defined nanostructures [184]. The obtained CZTS nanoparticles displayed strong photoabsorption properties in the whole visible region, and the morphology of the particles has a major influence on the absorption of light properties (i.e. CZTS microparticles with a hierarchical structure showed improved absorption than the single plate-shaped particles stacked). An increase in the absorption of light by the hierarchical architecture can be because of an improvement in the optical path, allowing light to be captured more efficiently by scattering over the nanoplates network. The doughnut-shaped CZTS particles had a bandgap of 1.54 eV, and this agrees well with values reported in the literature [185,186] and showed its potential as a solar cell absorber. As secondary phases like ZnS (3.6 eV) and Cu_2SnS_3 (0.96 eV) would increase and decrease the CZTS particles bandgap, respectively, their possible existence can be ruled out.

Shin et al. [187] evaluated the effect of varying the Cu content from 0.01 to 0.025 M on the morphological, chemical, compositional, structural, and optical properties of CZTS nanoparticles. The findings of XRD, XPS, and TEM showed the presence of numerous broad peaks in the precursor powder that may well not be attributed to CZTS, $Cu_{2-x}S$, Sn_2S_3, ZnS, and Cu_2SnS_3, respectively. Nevertheless, apart from that produced at a copper concentration of 0.02 M, both kesterite CZTS and copper and tin-related secondary phases were present in the sulfurized nanoparticles. Inductively coupled plasma (ICP) findings revealed that the copper present in the sulfurized CZTS NPs increased from 16.57% to 32.94% as copper concentration increases while zinc and tin in the sulfurized CZTS NPs reduced with an increase in concentration of copper. UV–vis spectroscopy findings disclosed that in the visible region, the absorption coefficient of the sulfurized CZTS NPs was above 10^4 cm^{-1} and the sulfurized CZTS NP's bandgap energy decreases to 1.28 from 1.65 eV with an increase in copper concentration (Fig. 19).

CZTS nanocrystals with a flowerlike morphology were prepared from chloride salts and thiourea by microwave-assisted solvothermal synthesis [195]. The dried powder was further annealed for 30 min at 500 °C under constant flow of argon maintained at a flow rate of 50 mL/min. XRD pattern confirmed pure phase kesterite for both the as synthesized and the annealed. The XRD peaks of the annealed were sharp and intense compared to the unannealed nanocrystals. The creation of a single-phase CZTS was also substantiated by Raman spectra. A nearly dispersed flowerlike particles with a wavelength ranging from 400 to 800 nm in diameter were revealed in the SEM image. The magnified image of a single CZTS particle revealed that the flowerlike particle was made up of sheets that were orderly connected to one other to form the flowerlike particle. The atomic ratio of Cu:Zn:Sn:S was 2.24:0.76:1.07:3.9 in the energy dispersive X-Ray (EDX) study of the synthesized CZTS particles, which is very comparable to the theoretical value of 2:1:1:4. TEM image also confirmed the flowerlike morphology of the synthesized CZTS nanocrystals, and the crystallite size was found to vary between 10 and 15 nm, which is agrees with 17 nm calculated from the XRD data using Scherrer's formula. Selected Area Electron Diffraction (SAED) pattern was also consistent with the XRD data.

Pinto and co-workers [177] recently used microwave-assisted solvothermal method for synthesizing CZTS nanocrystals formed in ethylene glycol from thiourea and metal salts in the presence of different sources of excess other than thiourea. They also investigated the impact of varying the temperature of the synthesis, the influence of changing the copper and tin oxidation states. They found out that kesterite and wurtzite phase CZTS was formed in all the synthesized nanocrystals and that the ratio of kesterite to wurtzite phases is dependent on the excessive sulfur source, oxidation number of Sn, and on the ratio of sulfur to metal used in the synthesis. They showed that when an amino group is contained in the source of excess sulfur, an intermediate of Zn–Sn was formed which allowed for the variation in the phases of CZTS between kesterite and wurtzite through the initial valency state of tin (Sn) and the sulfur-to-metal ratio. When an amino group is contained in the source of excess sulfur, wurtzite phase formation was favored with CZTS synthesized using Sn (II) salts and low sulfur to metal ratio, while CZTS synthesized using high sulfur-to-metal ratio greater than four favored the formation of kesterite phase and

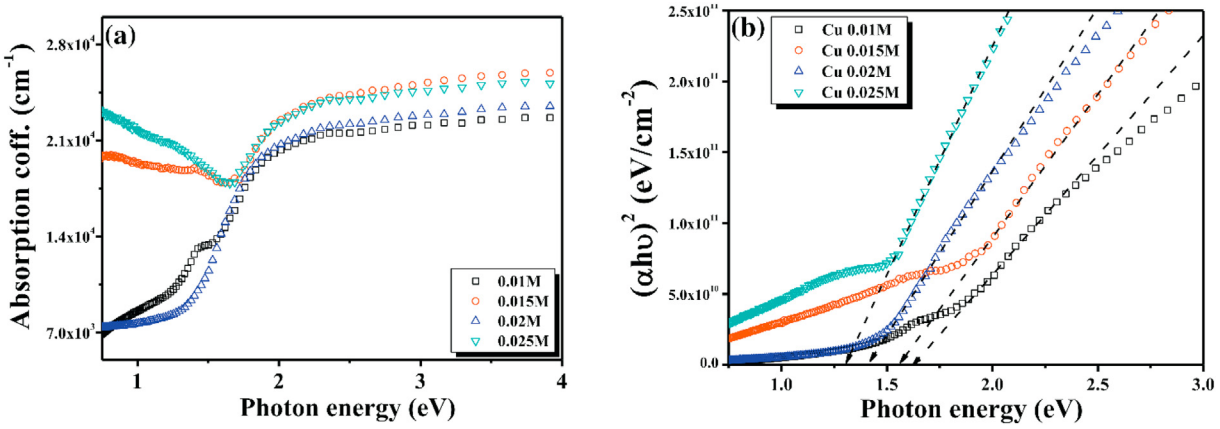

Fig. 19. (a) Optical absorption coefficient (b) $(\alpha h\upsilon)^2$ versus photon energy (hv) plot of the sulfurized CZTS NCs synthesized with various Cu concentration [Copyright with permission from Elsevier] [187].

Table 2
Summary of preparation method, optical, and physical properties of microwave synthesized CZTS nanoparticles.

solvents	Cation and anion source	Reaction conditions	Size(nm)	Bandgap	Ref
EG	$CuCl_2.2H_2O$, $ZnCl_2.H_2O$, $SnCl_2.2H_2O$, thiourea	800 W, 200 °C 1 h	14.9–18.7	1.27–1.54	[188]
DMF	$CuCl_2.2H_2O$, $ZnCl_2$, $SnCl_4.5H_2O$, thiourea, PVP as stabilizer	800 W, cyclic irradiation for 50 cycles	9	1.54	[183]
OLA	$Cu(acac)_2$, $Zn(acac)_2$, Sn bis$(acac)_2.Cl_2$, S powder	265 °C 15 min	20.2–38.9	1.46–1.5	[179]
EG	$CuCl_2.2H_2O$, $ZnCl_2.2H_2O$, $SnCl_2.2H_2O$, thiourea	700 W, 170–200 °C, 1 h	140–310	1.35–1.58	[130]
EG	$Cu(NO_3)_2$, $Zn(CH_3COO)_2$, $SnCl_2.2H_2O$, thiourea	10 min	300	1.5	[189]
EG	CuCl, $ZnCl_2$, $SnCl_4.5H_2O$, thiourea	180 °C, 30 min	17	1.67	[190]
EG	Copper (II) acetate monohydrate, tin (IV) chloride dehydrate, zinc acetate dihydrate, thiourea, PVP	150 °C, 1 h	N/A	1.49	[191]
EG	$Zn(CH_3COO)_2$, $SnCl_2.2H_2O$, $Cu(NO_3)_2$, thiourea, PVP	800 W, several min	150–350	1.4–1.62	[192]
EG	$CuCl_2.2H_2O$, $ZnCl_2.2H_2O$, $SnCl_2.2H_2O$, thiourea	800 W, 140–300 °C 5–20min	4.94–6.47	1.44–1.54	[193]
EG	$CuCl_2.2H_2O$, $ZnCl_2.2H_2O$, $SnCl_2.2H_2O$, thiourea, PVP	700 W, 200 °C 1 h	9.64	1.58	[194]
EG	$CuAc_2.H_2O$, CuAc, $ZnAc_2.2H_2O$, $SnCl_2$, $SnCl_4.5H_2O$, thiourea, L-cysteine, thioglycolic acid, 3-mercaptopropionic acid	300 W, 75–160 °C	3.7–6.4	N/A	[177]
EG	CuCl, $ZnCl_2$, $SnCl_4.5H_2O$, thioacetamide	300 W, 190 °C, 30 min	7.3–26.8	1.5	[110]
OLA TOPO	$Cu(acac)_2$, $Zn(OAc)_2$, $Sn(OAc)_4$, Sulfur powder.	700 W, 10 min	2.4–21	1.48–3.0	[41]

EG - ethylene glycol, DMF - dimethylformamide, OLA – oleylamine, TOPO – trioctylphosphine oxide.

when Sn (IV) salts was used, only the kesterite phase was obtained irrespective of the ratio of sulfur to metal. When an amino group was not present in the source of excess sulfur, wurtzite phase was the only phase formed under all the conditions investigated, irrespective of the valency of the Sn precursor or the ratio of sulfur to metal and in such situations, the intermediate Zn–Sn was not formed, and copper sulfide is the precursor to wurtzite phase. The sizes of the nanocrystals were found to be in the range of 3.7 and 6.4 nm, and it decreases with an increase in sulfur to metal ratio. The nanocrystals containing predominantly kesterite had the lowest average crystallite size. TEM images of the nanocrystals revealed that some nanocrystals were more spheroidal, while others were anisotropic oblate. Other authors in the literature have observed the anisotropic oblate nanocrystal when there was wurtzite CZTS [196]. The two distinct morphological patterns seen support the XRD findings, which showed that the produced nanocrystals were a mixture of wurtzite and kesterite CZTS and that the oblate shape was related with wurtzite CZTS, while the spherical shape was linked with kesterite CZTS. The selected area electron diffraction patterns exhibited rings with d-spacings which is compatible with the wurtzite as well as the kesterite phases. Table 2 summarizes some of the properties of CZTS synthesized by microwave method.

Despite the numerous advantages of microwave irradiation such as uniform heating, short heating period, high selectivity, faster reaction rates, and high efficiency over other fabrication methods [110,183], only few papers on the CZTSSe absorber via microwave synthetic route have been reported. It generally involves synthesis of CZTS nanoparticles by microwave irradiation, making an ink by dispersing the nanoparticles in a solvent and then spin coating the ink on a soda lime glass and dried on a hot plate to eliminate volatile solvents. The spin coating and drying method is repeated numerous times to reach the desired thickness, subsequent to annealing at high temperature in the presence of sulfur or selenide source.

In early work, Flynn et al. [110] fabricated thin film by spin coating ultrasonicated CZTS nanoparticles dispersed in ethylene glycol on a borosilicate glass substrate at 300 rpm for 10 s, then at 1500 rpm for 30 s. To remove volatile solvents, the substrate was placed on a hotplate at 80 °C after each coating and subsequently annealed for 20 min using 800 mg of tin (ii) sulfide and sulfur powder in the presence of flowing nitrogen at a temperature of 400 °C. CBD was used to deposit an n-type buffer layer of CdS (50 nm) on the CZTS annealed nanoparticle film. Window layers of 80 nm of i-ZnO and 300 nm of Al:ZnO were coated by sputtering. Numerous devices having an area of 0.07 cm^2 were seperated by mechanical scribing. Lastly, silver paste was applied as the top contacts. The fabricated solar cell had a final architecture of glass/Mo/CZTS/CdS/i-ZnO/Al:ZnO/Ag. The fabricated solar cell device gave a V_{OC} of 289 mV, a J_{SC} of 1.79 mA/cm^2, *FF* of 47.9%, and a PCE of 0.25%. The reason for the low efficiency could be because the cell suffered from a very low photocurrent. Another reason could be because of the borosilicate substrate glass used as majority of kesterite researchers employed soda lime molybdenum glass as the sodium has been shown to increase the efficiency and reliability of PV cells as well as tolerance [132,133].

Chen et al. [41] fabricated a CZTSSe solar cell from nanoparticles synthesized by microwave irradiation from the same volume of a mixed solvent of oleylamine (OLA) and trioctylphospine oxide (TOPO); 150 mg of the nanoparticles were dispersed in 1 ml of hexanethiol to create a stable ink. The deposition was performed in a N_2-filled GB, the ink was directly spin-coated on molybdenum coated soda lime glass substrate and was heated using a hot plate for 2 min at 450 °C to eliminate solvent and any other volatile molecules. The procedure was performed several times to obtain a CZTS thin film with 1.2 m thickness. 90 mg of Sn and 300 mg of elemental selenium were placed in a graphite box together with the as-coated substrates to suppress the loss of surface Sn-related species (such as SnS and SnSe) in order to obtain the CZTSSe thin-film and annealed in a quartz tube furnace with Ar flow at 575 °C for 12 min. The CZTSSe thin film was etched by KCN and the solar cell was made by the deposition of 50 nm CdS via CBD and thereafter intrinsic ZnO (50 nm) and In_2O_3:Sn (300 nm) were fabricated by rf-magnetron sputtering. The PV cell had a V_{OC} of 360 mV, a J_{SC} of 29.1 mA/cm^2, *FF* of 42.77% and an η of 4.48% which is currently the champion efficiency for a microwave route to CZTSSe solar cell device (Fig. 20). There is a massive improvement in the PCE compared to that reported by Flynn et al. [110] and the reason is not farfetched because CZTSSe absorbers holds the world record efficiency of 12.6% and Se being a better transport agent than S, it is expected to have a higher efficiency compared to that of CZTS. Another reason for the improvement is that soda lime glass was used as the substrate in place of borosilicate used by Flynn and coworker [110] and also the CZTSSe absorber were etched before

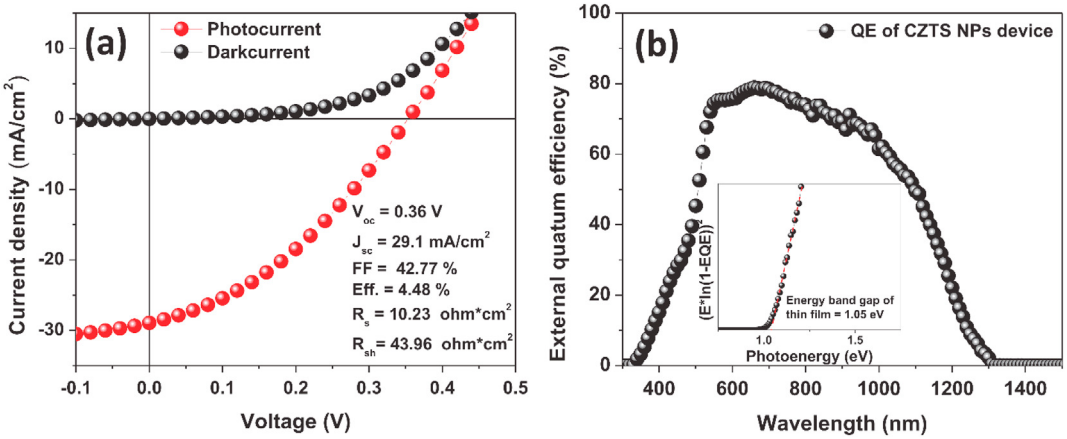

Fig. 20. (a) I–V parameters of the champion solar cell device fabricated using selenized CZTS NPs inks absorber made by microwave-assisted method under AM 1.5 illumination (b) External quantum efficiency curve of the champion solar cell and selenized CZTS bandgap as shown in the inset is deduced from the EQE spectrum [Copyright with permission from Elsevier] [41].

CBD of CdS, and etching has been shown by several authors to help in the removal of secondary phases that may be detrimental to the solar cell thereby improving the efficiency [82].

The only existing report in the literature that fabricated superstrate CZTS TFSC using microwave route was reported by Vahid and Salimeh [156]. They fabricated a superstrate thin film Cu_2ZnSnS_4 solar cell free of cadmium on a flexible substrate by making use of a nanocrystal ink obtained by microwave synthesis. ZnO nanorods arrays were hydrothermally grown on ITO substrate with nutrient solution containing 0.001 M of zinc nitrate hexahydrate and 0.1 M sodium hydroxide at 70 °C for 90 min. Prior to the formation of ZnO nanorods, a thin film of the seed layer ZnO have been applied on the ITO substrate via RF magnetron sputtering method. The nanocrystals obtained from the microwave synthesis were used to form an ink by dispersing in toluene, and it was dropped onto the ZnO nanorods (buffer layer) and dried for 6 h at room temperature. To construct the CZTS superstrate type thin film solar cell, carbon adhesive tape was used for hole collection on the absorbent layer. The fabricated solar cell had a final configuration of glass/ITO/ZnO nanorods/CZTS/carbon and the cell's EQE exhibited a maximum of about 57% at 532 nm. Fig. 21 (a and b) shows the vertically aligned ZnO and the I–V characteristics of the device. The device had a V_{OC} of 405 mV, a J_{SC} of 4.35 mA/cm^2, *FF* of 46.9%, and an η of 0.83%.

7. Challenges and future outlook

Synthesis and fabrication of CZTS solar cell by microwave and CZTS superstrate solar cells are still under investigated and an

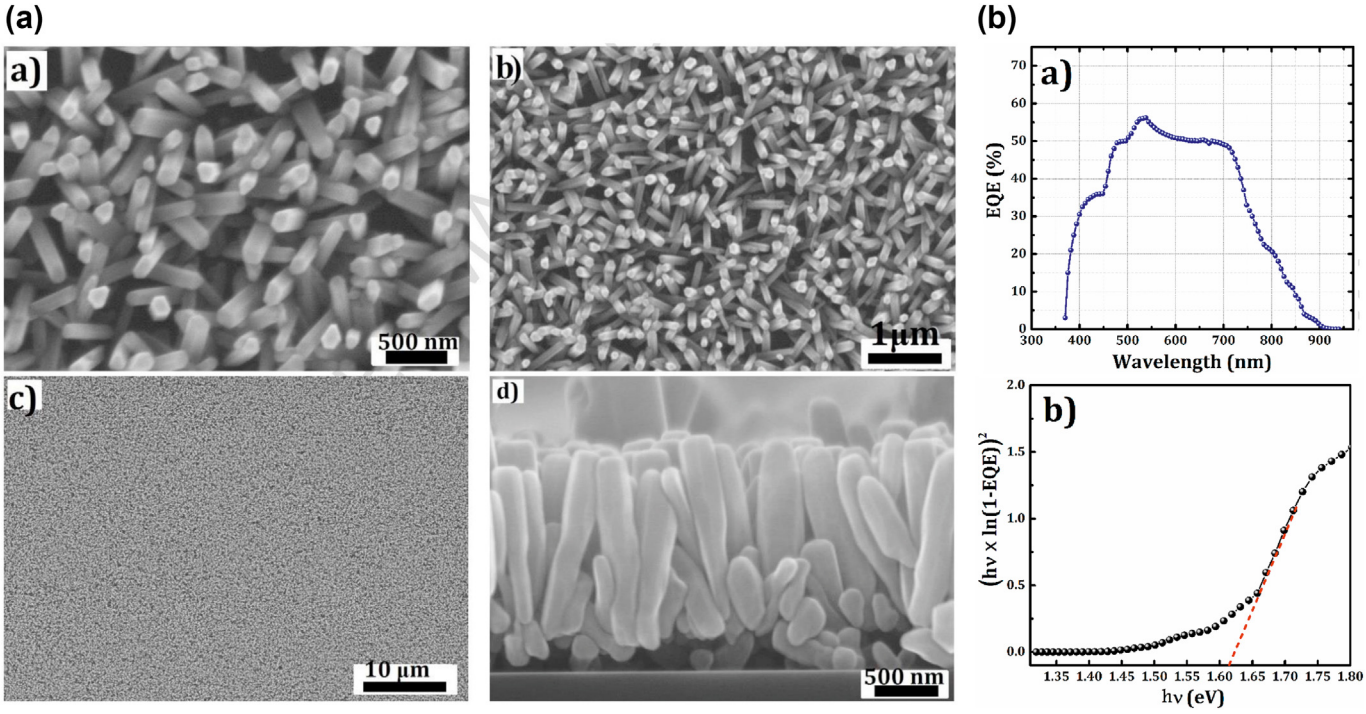

Fig. 21. a: SEM images of ZnO nanorod arrays grown vertically on ITO substrate [Copyright with permission from Elsevier] [156]. **b:** (a). EQE versus wavelength and (b) Tauc plot for the calculation of the bandgap of the absorber [Copyright with permission from Elsevier] [156].

effort to improve on the efficiency is still ongoing. Although remarkable advancement have been made in obtaining higher PV efficiencies for superstrate solar cell based on CZTS as well as microwave route to CZTS thin film solar cells but the reported efficiency (η) of the best device still does not match the efficiency of about 31% estimated theoretically and lags behind that of the substrate configuration and has yet to see any major improvement of above 4% in recent times [41,134,197,198]. The best efficiency reported for CZTS superstrate solar cell is 3.63% with a V_{OC} of 868.9 mV, a *Jsc* of 8.5 mA/cm^2, and *FF* of 49.1% and that obtained via microwave route has an η of 4.48%, a V_{OC} of 360 mV, *Jsc* of 29.1 mA/cm^2, and *FF* of 42.77% compared to an η of 12.6%, *Voc* of 513.4 mV, *Jsc* of 35.2 mA/cm^2, *FF* of 69.8% and a recently certified η of 12.96%, a V_{OC} of 529 mV, *Jsc* 33.58 mA/cm^2, and a *FF* of 69.8% for the substrate configuration, which are the champion and the best efficiency reported so far for CZTSSe thin film solar cells [41,52,128,129]. The major focus should be tailored toward improving the V_{OC} and *FF*. In general, controlling the quaternary chemical composition, favorable composition, morphology, particle size, use of toxic solvents, capping agents and surfactants under extreme conditions, green synthesis [105], obtaining a single phase since the single phase exists in a very confined area of the phase diagram, secondary phases formation, point defects, and open-circuit voltage deficit [21] are some of the challenges in synthesis and fabrication of substrate/superstrate CZTS/Se that has led to the stagnancy of PCEs at less than 13% despite the early rapid growth achieved with record efficiency between 2010 and 2014 [197]. Microwave synthetic and fabrication route to CZTS solar cells have numerous advantages such as uniform heating, short heating period, high selectivity, faster reaction rates, and high efficiency over other fabrication methods which offer a scalable route to the production of cost-effective solar cell absorber. The superstrate configuration is a promising configuration to compete with the substrate configuration as it combine the advantages of nanostructures with that of a thin film, and it has been proved to improve the conversion efficiencies of thin film solar cells and the metal oxide nanostructures due to their controllable dimensions and aligned morphologies have been shown to generate charges more efficiently, collect, and transfer charges efficiently as a result of the wide junction area and the narrow distance of collection to the interface. Irrespective of the type of configuration used or method of synthesis used for CZTS fabrication, it is a consensus among kesterite researchers that the V_{OC} is the key factor limiting kesterite-based thin film solar cells (TFSCs) though the origin still remains an open debate among researchers. We hypothesize that the following reason is responsible for the V_{OC} deficit (1) ITO/nanostructures used to block and facilitate the photogeneration of charge carriers are not properly optimized leading to a high recombination velocity thereby invariably leading to a high V_{OC} deficit. (2) Poor optimization of the p-n interface between the CdS buffer layers and CZTS leads to rapid electron hole recombination, implying that the buffer layer thickness should be regulated. (3) Defects and disorders are easily produced in the majority of the CZTS absorber layer, decreasing lifetimes of minority charge carriers and improving recombination [21]. In addition to the V_{OC} deficit, large series resistance, low shunt resistance, low fill factor, non-stoichiometric composition, severe holes and cracks at higher temperatures, faster electron–hole recombination at the junction, poor crystal quality, non-uniformity of the films, low temperature procedures involved in the annealing process does not allow for grain growth, non-post-annealing in sulfur or selenide environment involved in the manufacture of CZTS superstrate solar cells results in poor quality film thus enhancing recombination thereby resulting in poor solar cell device performance.

To increase the V_{OC}, the concentration of Cu_{Zn} antisite defects resulting from Cu and Zn intermixing must be decreased and one way to achieve that is by substituting other large-size elements/atoms for Zn or Cu, which could probably prevent the formation of defects and thereby improving the sample quality, so developing alternative novel materials is essential in improving the performance of CZTS superstrate solar cell [199–202]. Identification of an activation process for kesterite comparable to CdTe that helps to passivate the grain boundaries and enlarge the grain size may offer promising steps toward improving on the PV action of kesterite. Different growth processes have been reported which makes comparison of physical properties complicated so it therefore imperative that device measurement that concerns carrier generation, transport, and recombination must be accurately and consistently measured which may offer helpful information to overcoming the device drawbacks. Simulation of the materials and more precise techniques for local structure could help solve the problem of quantifying defects and disorder as techniques that are being used in the literature such as Raman spectroscopy, optical spectroscopy, and neutron diffraction do not provide valuable information into the distribution of microscopic cations that interact with the photogenerated electrons and holes [21]. In addition to the aforementioned, for a superstrate CZTS solar cell optimizing the deposition process, controlling the stoichiometry, controlling the morphology, employing compatible metallic top contacts, varying the aspect ratio of the window layer nanostructures, alternative buffer layers apart from CdS and ZnS that can withstand high temperature and probably reduce the interdiffusion of buffer layer at higher temperatures, which could lead to the disruption of CZTS/buffer interface should also be investigated, doping of CZTS with metals, and employing it in a hybrid inorganic–organic solar cell. Identifying other alternative device architecture (tandem) is some of the possible ways of enhancing the PV performance. Another way suggested to improve the device efficiency is by annealing in an environment containing sulfur or selenium so as to obtain high-quality crystals.

8. Conclusion

It is critical to find an alternative sources of energy to fossil fuels as it will eventually reduce with time. Lately, efforts have been geared toward thin film-based solar energy generation as it provides the most probable solution to large-scale energy generation. In recent years, research into CZTS thin film absorber have been heightened due to its unique characteristics such as environmental friendliness, natural abundance, high absorption coefficient, and tunable bandgap. However, the performance of the best CZTS solar cell device is still stalled at less than 13%, and for it to be widely and commercially accepted, it must have reached an efficiency of above 15% in the laboratory. Two different device architectures are commonly employed for the production of CZTS solar cell devices: the substrate and superstrate configuration. The advantages of the superstrate configuration over the substrate configuration have been exploited to fabricate high efficiency CZTS solar cell devices; however, the efficiency is still lower than that of the substrate configuration. In this paper, we reviewed some of the physical properties of CZTS such as the crystal structure, electronic properties, defects, and secondary phases; the different techniques for the synthesis of CZTS were also summarized, the CZTS device architecture in both the substrate and superstrate configuration was also summarized, discussed the working principle of CZTS solar cell, the techniques used for fabrication of CZTS superstrate solar cells have been reviewed. Microwave synthesis and characterization

of CZTS was also reviewed and the impact of variables such as temperature, surfactant, and reagents on their physical properties as well as the methods used in fabricating CZTS TFSC in the literature by the microwave route. We summarize the various challenges of CZTS solar absorber materials and the future prospects in order to help CZTS researchers focus on how to easily tailor their research on improving the device architecture. Despite being rarely studied microwave and superstrate CZTS thin film solar devices have achieved an efficiency of over 4% and when CZTS was doped with lithium and used as a hybrid solar cell an efficiency of over 5% was achieved. This shows that microwave synthetic route and superstrate device architecture is a promising aspect of CZTS that could be explored to compete with other route to synthesizing CZTS and the substrate configuration and its advantages such as cheap cost involved in its production and simple processes of manufacture allows for the production of electricity at a low cost.

Data availability

The authors are unable or have chosen not to specify which data has been used.

Declaration of competing interest

The authors declare that they have no known competing financial interests or personal relationships that could have appeared to influence the work reported in this paper.

Acknowledgments

This work was funded by research grants awarded by the National Research Foundation (NRF) of South Africa: (i) the Blue Skies Research Programme Grant No.: 110981; and (ii) the South African Research Chair Initiative (SARChI) Grant No.: 85102.

References

[1] I.M. Bugaje, Renewable energy for sustainable development in Africa: a review, Renew. Sustain. Energy Rev. 10 (6) (2006) 603–612, https://doi.org/10.1016/j.rser.2004.11.002.
[2] A. Demirbas, Global renewable energy projections, Energy Sources, Part B Econ. Plan. Policy 4 (2) (2009) 212–224, https://doi.org/10.1080/15567240701620499.
[3] I. Yüksel, Hydroelectric power in developing countries, Energy Sources, Part B Econ. Planning, Policy 4 (4) (Oct. 2009) 377–386, https://doi.org/10.1080/15567240701756897.
[4] T.M.H. Dabros, M.Z. Stummann, M. Hoj, P.A. Jensen, J.-D. Grunwaldt, J. Gabrielsen, P.M. Mortensen, A.D. Jensen, Transportation fuels from biomass fast pyrolysis, catalytic hydrodeoxygenation, and catalytic fast hydropyrolysis, Prog. Energy Combust. Sci. 68 (Sep. 01, 2018) 268–309, https://doi.org/10.1016/j.pecs.2018.05.002. Elsevier Ltd.
[5] M.A. Deshmukh, S.J. Park, B.S. Hedau, T.J. Ha, Recent progress in solar cells based on carbon nanomaterials, Sol energy 220 (May 15, 2021) 953–990, https://doi.org/10.1016/j.solener.2021.04.001. Elsevier Ltd.
[6] S.A. Khalate, R.S. Kate, R.J. Deokate, A review on energy economics and the recent research and development in energy and the Cu_2ZnSnS_4 (CZTS) solar cells: a focus towards efficiency, Sol. Energy 169 (Jul. 15, 2018) 616–633, https://doi.org/10.1016/j.solener.2018.05.036. Elsevier Ltd.
[7] F. Wang, J.D. Harindintwali, Z. Yuan, M. Wang, F. Wang, S. Li, Z. Yin, L. Huang, Y. Fu, L. Li, S.X. Chang, L. Zhang, J. Rinklebe, Z. Yuan, Q. Zhu, L. Xiang, D.C.W. Tsang, L. Xu, X. Jiang, J. Liu, N. Wei, M. Kästner, Y. Zou, Y.S. Ok, J. Shen, D. Peng, W. Zhang, D. Barceló, Y. Zhou, Z. Bai, B. Li, B. Zhang, K. Wei, H. Cao, Z. Tan, L.-B. Zhao, X. He, J. Zheng, N. Bolan, X. Liu, C. Huang, S. Dietmann, M. Luo, N. Sun, J. Gong, Y. Gong, F. Brahushi, T. Zhang, C. Xiao, X. Li, W. Chen, N. Jiao, J. Lehmann, Y.-G. Zhu, H. Jin, A. Schäffer, J.M. Tiedje, J.M. Chen, Technologies and perspectives for achieving carbon neutrality, Innovation 2 (4) (Nov. 28, 2021), 100180, https://doi.org/10.1016/j.xinn.2021.100180. Cell Press.
[8] O. Inganäs, V. Sundström, Solar energy for electricity and fuels, Ambio 45 (1) (Jan. 2016) 15–23, https://doi.org/10.1007/s13280-015-0729-6.
[9] Q. Dong, M. Chen, Y. Liu, F.T. Eickemeyer, W. Zhao, Z. Dai, Y. Yin, C. Jiang, J. Feng, S. Jin, S.F. Liu, S.M. Zakeeruddin, M. Gratzel, N.P. Padture, Y. Shi, Flexible perovskite solar cells with simultaneously improved efficiency, operational stability, and mechanical reliability, Joule 5 (6) (Jun. 2021) 1587–1601, https://doi.org/10.1016/j.joule.2021.04.014.
[10] N. Kannan, D. Vakeesan, Solar energy for future world: - a review, Renew. Sustain. Energy Rev. 62 (Sep. 01, 2016) 1092–1105, https://doi.org/10.1016/j.rser.2016.05.022. Elsevier Ltd.
[11] S. Kim, V.Q. Hoang, C.W. Bark, Silicon-based technologies for flexible photovoltaic (Pv) devices: from basic mechanism to manufacturing technologies, Nanomaterials 11 (11) (2021), https://doi.org/10.3390/nano11112944.
[12] A. Demirbas, Energy issues and energy priorities, Energy Sources, Part B Econ. Plan. Policy 3 (1) (2008) 41–49, https://doi.org/10.1080/15567240701548757.
[13] U. S. IEA, US energy information administration, international energy outlook 2017 overview, Int. Energy Outlook IEO2017 (2017) (2017) 143. www.eia.gov/forecasts/ieo/pdf/0484(2016).pdf.
[14] M.K.H. Rabaia, M.A. AbdelKareem, E.T. Sayed, K. Elsaid, K.J. Chae, T. Wilberforce, A.G. Olabi, Environmental impacts of solar energy systems: a review, Sci. Total Environ. 754 (Feb. 2021) 141989, https://doi.org/10.1016/j.scitotenv.2020.141989.
[15] S. Zhuk, A. Kushwaha, T.K.S. Wong, S. Masudy-Panah, A. Smirnov, G.K. Dalapati, Critical review on sputter-deposited Cu_2ZnSnS_4 (CZTS) based thin film photovoltaic technology focusing on device architecture and absorber quality on the solar cells performance, Sol. Energy Mater. Sol. Cells 171 (November 2016) (2017) 239–252, https://doi.org/10.1016/j.solmat.2017.05.064.
[16] M. Jamil, M. Amami, A. Ali, K. Mahmood, N. Amin, Numerical modeling of AZTS as buffer layer in CZTS solar cells with back surface field for the improvement of cell performance, Sol. Energy 231 (Jan. 2022) 41–46, https://doi.org/10.1016/j.solener.2021.11.025.
[17] P.D. Matthews, P.D. McNaughter, D.J. Lewis, P. O'Brien, Shining a light on transition metal chalcogenides for sustainable photovoltaics, Chem. Sci. 8 (6) (2017) 4177–4187, https://doi.org/10.1039/c7sc00642j.
[18] K.L. Chopra, P.D. Paulson, V. Dutta, Thin-film solar cells: an overview, Prog. Photovoltaics Res. Appl. 12 (23) (2004) 69–92, https://doi.org/10.1002/pip.541.
[19] T.D. Lee, A.U. Ebong, A review of thin film solar cell technologies and challenges, Renew. Sustain. Energy Rev. 70 (September 2015) (2017) 1286–1297, https://doi.org/10.1016/j.rser.2016.12.028.
[20] M. Green, K. Emery, Y. Hishikawa, W. Warta, E. Dunlop, D. Barkhouse, O. Gunawan, T. Gokmen, T. Todorov, D. Mitzi, Solar cell efficiency tables (version 40), IEEE Trans. Fuzzy Syst. 20 (6) (2012) 1114–1129, https://doi.org/10.1002/pip.2909.
[21] S.K. Wallace, D.B. Mitzi, A. Walsh, The steady rise of kesterite solar cells, ACS Energy Lett. 2 (4) (2017) 776–779, https://doi.org/10.1021/acsenergylett.7b00131.
[22] R.B.V. Chalapathy, M.G. Gang, C.W. Hong, J.H. Kim, J.S. Jang, J.H. Yun, J.H. Kim, Performance of CZTSSe thin film solar cells fabricated using a sulfo-selenization process: influence of the Cu composition, Sol. Energy 159 (October 2017) (2018) 260–269, https://doi.org/10.1016/j.solener.2017.10.085.
[23] A. Hedibi, A. Gueddim, B. Bentria, Numerical modeling and optimization of ZnO:Al/iZnO/ZnMgO/CZTS photovoltaic solar cell, Trans. Electr. Electron. Mater. 1 (Jan. 2021) 3, https://doi.org/10.1007/s42341-020-00278-w.
[24] B.R. Bade, S.R. Rondiya, Y.A. Jadhav, M.M. Kamble, S.V. Barma, S.B. Jathar, M.P. Nasane, S.R. Jadkar, A.M. Funde, N.Y. Dzade, Investigations of the structural, optoelectronic and band alignment properties of Cu_2ZnSnS_4 prepared by hot-injection method towards low-cost photovoltaic applications, J. Alloys Compd. 854 (Feb. 2021) 157093, https://doi.org/10.1016/j.jallcom.2020.157093.
[25] S.R. Rondiya, Y.A. Jadhav, A. Živkovićc, S.B. Jathar, G.K. Rahane, R.W. Cross, A.V. Rokade, R.S. Devan, S. Kolekar, R.L.Z. Hoye, H.N. Ghosh, N.H. de Leeuw, S.R. Jadkar, N.Y. Dzade, Solution-processed Cd-substituted CZTS nanocrystals for sensitized liquid junction solar cells, J. Alloys Compd. 890 (2022), https://doi.org/10.1016/j.jallcom.2021.161575.
[26] H. Zhou, W.C. Hsu, H.S. Duan, B. Bob, W. Yang, C.J. Song, T. Bin, Hsu, Y. Yang, CZTS nanocrystals: a promising approach for next generation thin film photovoltaics, Energy Environ. Sci. 6 (10) (2013) 2822–2838, https://doi.org/10.1039/c3ee41627e.
[27] T.K. Todorov, K.B. Reuter, D.B. Mitzi, High-efficiency solar cell with earth-abundant liquid-processed absorber, Adv. Mater. 22 (20) (2010) 156–159, https://doi.org/10.1002/adma.200904155.
[28] W. Yang, H.S. Duan, B. Bob, H. Zhou, B. Lei, C.H. Chung, S.H. Li, W.W. Hou, Y. Yang, Novel solution processing of high-efficiency earth-abundant $Cu_2ZnSn(S,Se)_4$ solar cells, Adv. Mater. 24 (47) (2012) 6323–6329, https://doi.org/10.1002/adma.201201785.
[29] H. Katagiri, K. Jimbo, W.S. Maw, K. Oishi, M. Yamazaki, H. Araki, A. Takeuchi, Development of CZTS-based thin film solar cells, Thin Solid Films 517 (7) (2009) 2455–2460, https://doi.org/10.1016/j.tsf.2008.11.002.
[30] Q. Guo, H.W. Hillhouse, R. Agrawal, Synthesis of Cu2ZnSnS4 nanocrystal ink and its use for solar cells, J. Am. Chem. Soc. 131 (33) (2009) 11672–11673, https://doi.org/10.1021/ja904981r.
[31] S. Singh, A.K. Katiyar, A. Midya, A. Ghorai, S.K. Ray, Superior heterojunction properties of solution processed copper-zinc-tin-sulphide quantum dots on Si, Nanotechnology 28 (43) (2017), https://doi.org/10.1088/1361-6528/aa81dd.
[32] S. Kim, J.S. Park, A. Walsh, Identification of killer defects in kesterite thin-film solar cells, ACS Energy Lett. 3 (2) (2018) 496–500, https://doi.org/10.1021/acsenergylett.7b01313.

[33] S.P. Madhusudanan, M. Suresh Kumar, K. Mohanta, S.K. Batabyal, Photoactive Cu_2FeSnS_4 thin films: influence of stabilizers, Appl. Surf. Sci. 535 (Jan. 2021) 147600, https://doi.org/10.1016/j.apsusc.2020.147600.

[34] A.A. Ahmad, A.B. Migdadi, A.M. Alsaad, I.A. Qattan, Q.M. Al-Bataineh, A. Telfah, Computational and experimental characterizations of annealed Cu_2ZnSnS_4 thin films, Heliyon 8 (1) (Jan. 2022) e08683, https://doi.org/10.1016/j.heliyon.2021.e08683.

[35] A. Irkhina, S. Levcenko, V. Hinrichs, P. Plate, T. Unold, Metal acetate based synthesis of small-sized Cu2ZnSnS4 nanocrystals: effect of injection temperature and synthesis time, RSC Adv. 7 (19) (2017) 11752–11760, https://doi.org/10.1039/c6ra28588k.

[36] I. Gunes, V. Bilgin, E. Sarica, Non-stoichiometric effect and disorder in as-prepared Cu_2ZnSnS_4 films deposited at different temperatures by ultrasonic spray pyrolysis, Mater. Sci. Semicond. Process. 152 (Dec. 2022) 107120, https://doi.org/10.1016/j.mssp.2022.107120.

[37] S. Sengupta, R. Aggarwal, M. Raula, A review on chemical bath deposition of metal chalcogenide thin films for heterojunction solar cells, J. Mater. Res. (2022) 1–12, https://doi.org/10.1557/s43578-022-00539-9.

[38] M. Dhanasekar, S.V. Bhat, Facile synthesis of Cu_2ZnSnS_4 absorber layer for thin film solar cells using a highly stable precursor solution, Appl. Surf. Sci. 418 (2017) 194–198, https://doi.org/10.1016/j.apsusc.2016.12.227.

[39] S. Bag, O. Gunawan, T. Gokmen, Y. Zhu, T.K. Todorov, D.B. Mitzi, Low band gap liquid-processed CZTSe solar cell with 10.1% efficiency, Energy Environ. Sci. 5 (5) (2012) 7060–7065, https://doi.org/10.1039/c2ee00056c.

[40] H. Xin, J.K. Katahara, I.L. Braly, H.W. Hillhouse, 8% Efficient $Cu_2ZnSn(S,Se)_4$ solar cells from redox equilibrated simple precursors in DMSO, Adv. Energy Mater. 4 (11) (2014) 1–5, https://doi.org/10.1002/aenm.201301823.

[41] W.C. Chen, V. Tunuguntla, M.H. Chiu, L.J. Li, I. Shown, C.H. Lee, J.S. Hwang, L.C. Chen, K.H. Chen, Co-solvent effect on microwave-assisted Cu_2ZnSnS_4 nanoparticles synthesis for thin film solar cell, Sol. Energy Mater. Sol. Cells 161 (1) (2017) 416–423, https://doi.org/10.1016/j.solmat.2016.12.013.

[42] L. Guo, Y. Zhu, O. Gunawan, T. Gokmen, V.R. Deline, S. Ahmed, L.T. Romankiw, H. Deligianni, Electrodeposited $Cu_2ZnSnSe_4$ thin film solar cell with 7% power conversion efficiency, Prog. Photovolt: Res. Appl. 22 (2014) 58–68. https://doi.org/10.1002/pip.2332.

[43] V. Minh, J. Bae, J. Shim, B. Hong, H. Jee, J. Lee, Fabrication of the Cu_2ZnSnS_4 thin film solar cell via a photo-sintering technique, Appl. Sci. 12 (2022) 38.

[44] S.A. Vanalakar, P.S. Patil, J.H. Kim, Recent advances in synthesis of Cu_2FeSnS_4 materials for solar cell applications: a review, Sol. Energy Mater. Sol. Cells 182 (March) (2018) 204–219, https://doi.org/10.1016/j.solmat.2018.03.021.

[45] R. Anne Sarah Christinal, I. Prakash, S. Chakravarty, A. Leo Rajesh, Spray pyrolysed Cu_2ZnSnS_4 thin film photovoltaic cell fabricated using cost effective materials, Phys. B Condens. Matter 637 (Jul. 2022) 413911, https://doi.org/10.1016/j.physb.2022.413911.

[46] I. Bilecka, M. Niederberger, Microwave chemistry for inorganic nanomaterials synthesis, Nanoscale 2 (8) (2010) 1358–1374, https://doi.org/10.1039/b9nr00377k.

[47] C.O. Kappe, Controlled microwave heating in modern organic synthesis, Angew. Chem., Int. Ed. 43 (46) (2004) 6250–6284, https://doi.org/10.1002/anie.200400655.

[48] B.L. Hayes, "Brittany L. Hayes-Microwave Synthesis_ Chemistry at the Speed of Light-Cem Corp (2002).pdf.", 2002.

[49] M.B. Schütz, L. Xiao, T. Lehnen, T. Fischer, S. Mathur, Microwave-assisted synthesis of nanocrystalline binary and ternary metal oxides, Int. Mater. Rev. 63 (6) (2018) 341–374, https://doi.org/10.1080/09506608.2017.1402158.

[50] M.P. Paranthaman, W. Wong-Ng, R.N. Bhattacharya, Semiconductor Materials for Solar Photovoltaic Cells, vol. 4, 2015.

[51] R. Yan, L. Kang, Y. Sun, J. Zhang, Solution-processed Cu_2ZnSnS_4 thin film with mixed solvent and its application in superstrate structure solar cells, RSC Adv. 8 (21) (2018) 11469–11477, https://doi.org/10.1039/c8ra01095a.

[52] A. Ghosh, R. Thangavel, A. Gupta, Solution-processed Cd free kesterite Cu_2ZnSnS_4 thin film solar cells with vertically aligned ZnO nanorod arrays, J. Alloys Compd. 694 (2017) 394–400, https://doi.org/10.1016/j.jallcom.2016.09.325.

[53] V. V Rakitin, G.F. Novikov, Third-generation solar cells based on quaternary copper compounds with the kesterite-type structure, Russ. Chem. Rev. 86 (2) (2017) 99–112, https://doi.org/10.1070/rcr4633.

[54] A. Walsh, S. Chen, S.H. Wei, X.G. Gong, Kesterite thin-film solar cells: advances in materials modelling of Cu_2ZnSnS_4, Adv. Energy Mater. 2 (4) (2012) 400–409, https://doi.org/10.1002/aenm.201100630.

[55] Z. Shi, D. Attygalle, A.H. Jayatissa, Kesterite-based next generation high performance thin film solar cell: current progress and future prospects, J. Mater. Sci. Mater. Electron. 28 (2) (2017) 2290–2306, https://doi.org/10.1007/s10854-016-5753-1.

[56] S. Chen, X.G. Gong, A. Walsh, S.H. Wei, Crystal and electronic band structure of Cu_2ZnSnX_4 (X=S and Se) photovoltaic absorbers: first-principles insights, Appl. Phys. Lett. 94 (4) (2009) 94–97, https://doi.org/10.1063/1.3074499.

[57] A.J. Jackson, A. Walsh, Abinitio thermodynamic model of Cu_2ZnSnS_4, J. Mater. Chem. 2 (21) (2014) 7829–7836, https://doi.org/10.1039/c4ta00892h.

[58] A. Khare, B. Himmetoglu, M. Johnson, D.J. Norris, M. Cococcioni, E.S. Aydil, Calculation of the lattice dynamics and Raman spectra of copper zinc tin chalcogenides and comparison to experiments, J. Appl. Phys. 111 (8) (2012), https://doi.org/10.1063/1.4704191.

[59] S. Siebentritt, S. Schorr, Kesterites-a challenging material for solar cells, Prog. Photovoltaics Res. Appl. 20 (5) (Aug. 2012) 512–519, https://doi.org/10.1002/pip.2156.

[60] S. Schorr, H.-J. Hoebler, M. Tovar, A neutron diffraction study of the stannite-kesterite solid solution series, Eur. J. Mineral 19 (1) (2007) 65–73, https://doi.org/10.1127/0935-1221/2007/0019-0065.

[61] S. Schorr, The crystal structure of kesterite type compounds: a neutron and X-ray diffraction study, Sol. Energy Mater. Sol. Cells 95 (6) (2011) 1482–1488, https://doi.org/10.1016/j.solmat.2011.01.002.

[62] C. Persson, Electronic and optical properties of Cu_2ZnSnS_4 and $Cu_2ZnSnSe_4$, J. Appl. Phys. 107 (5) (2010), https://doi.org/10.1063/1.3318468.

[63] D.H. Friedlmeier Tm, N. Wieser, T. Walter, S. Hw, in: 14th European Photovoltaic Solar Energy Conference (Stephens and Asc., Barcelona) vol. 1, 1997, p. 1242.

[64] K.-H.K. Jae-Seung Seol, Sang-Yul Lee, Jae-Choon Lee, Hyo-Duk Nam, Electrical and optical properties of Cu_2ZnSnS_4 thin films prepared by rf magnetronsputtering process, Sol. Energy Mater. Sol. Cells 75 (2003) 155–162, https://doi.org/10.1016/S0927-0248(02)00127-7.

[65] L.V. Puyvelde, J. Lauwaert, P.F. Smet, S. Khelifi, T. Ericson, J.J. Scragg, D. Poelman, R.V. Deun, C. Platzer-Bjorkman, H. Vrielinck, Photoluminescence investigation of Cu_2ZnSnS_4 thin film solar cells, Thin Solid Films 582 (2015) 146–150, https://doi.org/10.1016/j.tsf.2014.10.079.

[66] G.K. Dalapati, S. Zhuk, S. Masudy-Panah, A. Kushwaha, H.L. Seng, V. Chellappan, V. Suresh, Z. Su, S.K. Batabyal, C.C. Tan, A. Guchhait, L.H. Wong, T.K.S. Wong, S. Tripathy, Impact of molybdenum out diffusion and interface quality on the performance of sputter grown CZTS based solar cells, Sci. Rep. 7 (1) (Dec. 2017), https://doi.org/10.1038/s41598-017-01605-7.

[67] T. Tanaka, T. Nagatomo, D. Kawasaki, M. Nishio, Q. Guo, A. Yoshida, H. Ogawa, Preparation of Cu_2ZnSnS_4 thin films by hybrid sputtering, J. Phys. Chem. Solid. 66 (11) (2005) 1978–1981, https://doi.org/10.1016/j.jpcs.2005.09.037.

[68] K. Moriya, J. Watabe, K. Tanaka, H. Uchiki, Characterization of Cu_2ZnSnS_4 thin films prepared by photo-chemical deposition, Phys. Status Solidi Curr. Top. Solid State Phys. 3 (8) (2006) 2848–2852, https://doi.org/10.1002/pssc.200669588.

[69] J.J. Scragg, P.J. Dale, L.M. Peter, Towards sustainable materials for solar energy conversion: preparation and photoelectrochemical characterization of Cu_2ZnSnS_4, Electrochem. Commun. 10 (4) (2008) 639–642, https://doi.org/10.1016/j.elecom.2008.02.008.

[70] N. Kamoun, H. Bouzouita, B. Rezig, Fabrication and characterization of Cu_2ZnSnS_4 thin films deposited by spray pyrolysis technique, Thin Solid Films 515 (15) (2007) 5949–5952, https://doi.org/10.1016/j.tsf.2006.12.144.

[71] K. Sekiguchi, K. Tanaka, K. Moriya, H. Uchiki, Epitaxial growth of Cu_2ZnSnS_4 thin films by pulsed laser deposition, Phys. Status Solidi Curr. Top. Solid State Phys. 3 (8) (2006) 2618–2621, https://doi.org/10.1002/pssc.200669603.

[72] J. Zhang, L. Shao, Y. Fu, E. Xie, Cu_2ZnSnS_4 thin films prepared by sulfurization of ion beam sputtered precursor and their electrical and optical properties, Rare Met. 25 (6 SUPPL. 1) (2006) 315–319, https://doi.org/10.1016/S1001-0521(07)60096-5.

[73] M. Altosaar, J. Raudoja, K. Timmo, M. Danilson, M. Grossberg, J. Krustok, E. Mellikov, $Cu_2Zn_{1-x}Cd_xSn(Se_{1-ySy})_4$ solid solutions as absorber materials for solar cells, Phys. Status Solidi Appl. Mater. Sci. 205 (1) (2008) 167–170, https://doi.org/10.1002/pssa.200776839.

[74] S. Ahn, S. Jung, J. Gwak, A. Cho, K. Shin, K. Yoon, D. Park, H. Cheong, J.H. Yun, Determination of band gap energy (Eg) of $Cu_2ZnSnSe_4$ thin films: on the discrepancies of reported band gap values, Appl. Phys. Lett. 97 (2) (2010), https://doi.org/10.1063/1.3457172.

[75] S. Chen, A. Walsh, X.G. Gong, S.H. Wei, Classification of lattice defects in the kesterite Cu_2ZnSnS_4 and $Cu_2ZnSnSe_4$ earth-abundant solar cell absorbers, Adv. Mater. 25 (11) (2013) 1522–1539, https://doi.org/10.1002/adma.201203146.

[76] M. Kumar, A. Dubey, N. Adhikari, S. Venkatesan, Q. Qiao, Strategic review of secondary phases, defects and defect-complexes in kesterite CZTS-Se solar cells, Energy Environ. Sci. 8 (11) (2015) 3134–3159, https://doi.org/10.1039/c5ee02153g.

[77] S. Chen, X.G. Gong, A. Walsh, S.H. Wei, Defect physics of the kesterite thin-film solar cell absorber Cu_2ZnSnS_4, Appl. Phys. Lett. 96 (2) (2010) 4–7, https://doi.org/10.1063/1.3275796.

[78] S. Chen, J.H. Yang, X.G. Gong, A. Walsh, S.H. Wei, Intrinsic point defects and complexes in the quaternary kesterite semiconductor Cu_2ZnSnS_4, Phys. Rev. B - Condens. Matter Mater. Phys. 81 (24) (2010) 35–37, https://doi.org/10.1103/PhysRevB.81.245204.

[79] D.M. Alex Polizzotti, Ingrid Repins, Rommel Noufi, Su-Huai Weib, The state and future prospects of kesterite photovoltaics, Energy Environ. Sci. 6 (2013) 3171–3182, https://doi.org/10.1039/C3EE41781F.

[80] J. Just, D. Ltzenkirchen-Hecht, R. Frahm, S. Schorr, T. Unold, Determination of secondary phases in kesterite Cu_2ZnSnS_4 thin films by x-ray absorption near edge structure analysis, Appl. Phys. Lett. 99 (26) (2011) 2011–2014, https://doi.org/10.1063/1.3671994.

[81] I.D. Olekseyuk, I.V. Dudchak, L.V. Piskach, Phase equilibria in the Cu_2S-ZnS-SnS_2 system, J. Alloys Compd. 368 (1–2) (2004) 135–143, https://doi.org/10.1016/j.jallcom.2003.08.084.

[82] H. Xie, Y. Sanchez, S. Lopez-Marino, M. Espindola-Rodriquez, M. Neuschitzer, D. Sylla, A. Fairbrother, V. Izquierdo-Roca, A. Perez-Rodriguez, E. Saucedo, Impact of Sn(S,Se) secondary phases in $Cu_2ZnSn(S,Se)_4$ solar cells: a chemical route for their selective removal and absorber surface passivation, ACS Appl. Mater. Interfaces 6 (15) (2014) 12744–12751, https://doi.org/10.1021/am502609c.

[83] Bao, W., & Ichimura, M. (2015). Influence of secondary phases in kesterite-cunSnSabsorber material based on the first principles calculation. *International Journal of Photoenergy*, *2015*(c). https://doi.org/10.1155/2015/592079

[84] S. Siebentritt, Why are kesterite solar cells not 20% efficient? Thin Solid Films 535 (1) (2013) 1–4, https://doi.org/10.1016/j.tsf.2012.12.089.
[85] V. Chawla, B. Clemens, Inexpensive, abundant, non-toxic thin films for solar cell applications grown by reactive sputtering, Conf. Rec. IEEE Photovolt. Spec. Conf. (2010) 1902–1905, https://doi.org/10.1109/PVSC.2010.5616337.
[86] C. Wang, L. Niare, B. Drame, Z. Ming, F.U. Yue-gang, Design and fabrication of new wide-band and wide-angle solar cell absorbing layer, Opt Laser. Technol. 134 (May 2020) (2021), 106588, https://doi.org/10.1016/j.optlastec.2020.106588.
[87] P. Fan, Z. Xie, G. Liang, M. Ishaq, S. Chen, Z. Zheng, C. Yan, J. Huang, X. Hao, Y. Zhang, Z. Su, High-efficiency ultra-thin Cu_2ZnSnS_4 solar cells by double-pressure sputtering with spark plasma sintered quaternary target, J. Energy Chem. (Jan. 2021), https://doi.org/10.1016/j.jechem.2021.01.026.
[88] N. Behera, D.B. Mohan, The phase optimization, optical and electrical properties of kesterite Cu_2ZnSnS_4 thin film prepared by single target RF magnetron sputtering technique for solar cell application, Mater. Res. Express 6 (12) (Feb. 2019) 126457, https://doi.org/10.1088/2053-1591/ab5e39.
[89] A. Redinger, D.M. Berg, P.J. Dale, S. Siebentritt, The consequences of kesterite equilibria for efficient solar cells, J. Am. Chem. Soc. 133 (10) (2011) 3320–3323, https://doi.org/10.1021/ja111713g.
[90] N. Khemiri, S. Chamekh, M. Kanzari, Properties of thermally evaporated CZTS thin films and numerical simulation of earth abundant and non toxic CZTS/Zn(S,O) based solar cells, Sol. Energy 207 (Sep. 2020) 496–502, https://doi.org/10.1016/j.solener.2020.06.114.
[91] S.W. Shin, S.M. Pawar, C.Y. Park, J.H. Yun, J.H. Moon, J.H. Kim, J.Y. Lee, Studies on Cu_2ZnSnS_4 (CZTS) absorber layer using different stacking orders in precursor thin films, Sol. Energy Mater. Sol. Cells 95 (12) (2011) 3202–3206, https://doi.org/10.1016/j.solmat.2011.07.005.
[92] K. Jimbo, R. Kimura, T. Kamimura, S. Yamada, W.S. Maw, H. Araki, K. Oishi, H. Katagiri, Cu_2ZnSnS_4-type thin film solar cells using abundant materials, Thin Solid Films 515 (15) (2007) 5997–5999, https://doi.org/10.1016/j.tsf.2006.12.103.
[93] X. Wu, W. Liu, S. Cheng, Y. Lai, H. Jia, Photoelectric properties of Cu_2ZnSnS_4 thin films deposited by thermal evaporation, J. Semiconduct. 33 (2) (2012), https://doi.org/10.1088/1674-4926/33/2/022002.
[94] H.S.T. Kato, H. Hiroi, N. Sakai, S. Muraoka, Characterization of front and back interfaces on Cu_2ZnSnS_4 thin-film solar cells, 27th Eur. Photovolt. Sol. Energy Conf. Exhib. (2012) 2236–2239, https://doi.org/10.4229/27thEUPVSEC2012-3CO.4.2.
[95] N. Sakai, H. Hiroi, H. Sugimoto, Development of Cd-free buffer layer for Cu_2ZnSnS_4 thin-film solar cells, in: Conference Record of the IEEE Photovoltaic Specialists Conference, 2011, pp. 3654–3657, https://doi.org/10.1109/PVSC.2011.6185941.
[96] G. Altamura, L. Grenet, C. Bougerol, E. Robin, D. Kohen, H. Fournier, A. Brioude, S. Perraud, H. Mariette, $Cu_2ZnSn(S_{1-x}Se_x)_4$ thin films for photovoltaic applications: influence of the precursor stacking order on the selenization process, J. Alloys Compd. 588 (2014) 310–315, https://doi.org/10.1016/j.jallcom.2013.11.068.
[97] L. Grenet, S. Bernandi, D. Kohen, C. Lepoittevin, S. Noel, N. Karst, A. Brioude, S. Perraud, H. Mariette, $Cu_2ZnSn(S_{1-x}Se_x)_4$ based solar cell produced by selenization of vacuum deposited precursors, Sol. Energy Mater. Sol. Cells 101 (2012) 11–14, https://doi.org/10.1016/j.solmat.2012.02.016.
[98] P.A. Fernandes, P.M.P. Salomé, A.F. Da Cunha, Study of polycrystalline Cu_2ZnSnS_4 films by Raman scattering, J. Alloys Compd. 509 (28) (2011) 7600–7606, https://doi.org/10.1016/j.jallcom.2011.04.097.
[99] P.A. Fernandes, P.M.P. Salome, A.F. Sartori, J. Malaquias, A.F. Da Cunha, B. Schubert, J.C. Gonzalez, G.M. Ribeiro, Effects of sulphurization time on Cu_2ZnSnS_4 absorbers and thin films solar cells obtained from metallic precursors, Sol. Energy Mater. Sol. Cells 115 (2013) 157–165, https://doi.org/10.1016/j.solmat.2013.03.032.
[100] J.C. González, P.A. Fernandes, G.M. Ribeiro, A. Abelenda, E.R. Viana, P.M.P. Salome, A.F. Da Cunha, Influence of the sulphurization time on the morphological, chemical, structural and electrical properties of Cu_2ZnSnS_4 polycrystalline thin films, Sol. Energy Mater. Sol. Cells 123 (2014) 58–64, https://doi.org/10.1016/j.solmat.2014.01.005.
[101] A.V. Moholkar, S.S. Shinde, G.L. Agawane, S.H. Jo, K.Y. Rajpure, P.S. Patil, C.H. Bhosale, J.H. Kim, Studies of compositional dependent CZTS thin film solar cells by pulsed laser deposition technique: an attempt to improve the efficiency, J. Alloys Compd. 544 (Dec. 2012) 145–151, https://doi.org/10.1016/j.jallcom.2012.07.108.
[102] K. Ramasamy, M.A. Malik, P. O'Brien, The chemical vapor deposition of Cu_2ZnSnS_4 thin films, Chem. Sci. 2 (6) (2011) 1170–1172, https://doi.org/10.1039/c0sc00538j.
[103] M.P. Suryawanshi, G.L. Agawane, S.M. Bhosale, S.W. Shin, P.S. Patil, J.H. Kim, A.V. Moholkar, CZTS based thin film solar cells: a status review, Mater. Technol. 28 (1–2) (2013) 98–109, https://doi.org/10.1179/1753555712Y.0000000038.
[104] M.I. Khalil, R. Bernasconi, L. Magagnin, CZTS layers for solar cells by an electrodeposition-annealing route, Electrochim. Acta 145 (2014) 154–158, https://doi.org/10.1016/j.electacta.2014.09.001.
[105] M. Karimi, M.J. Eshraghi, V. Jahangir, A facile and green synthetic approach based on deep eutectic solvents toward synthesis of CZTS nanoparticles, Mater. Lett. 171 (2016) 100–103, https://doi.org/10.1016/j.matlet.2016.02.065.
[106] R. Liu, M. Tan, X. Zhang, J. Chen, S. Song, W. Zhang, Impact of sol-gel precursor treatment with preheating temperature on properties of Cu_2ZnSnS_4 thin film and its photovoltaic solar cell, J. Alloys Compd. 655 (2016) 124–129, https://doi.org/10.1016/j.jallcom.2015.09.028.
[107] R. Ahmad, N.-H. Saddiqi, M. Wu, M. Prato, E. Spiecker, W. Peukert, M. Distaso, Effect of the counteranion on the formation pathway of Cu2ZnSnS4 (CZTS) nanoparticles under solvothermal conditions, Inorg. Chem. 59 (3) (2020) 1973–1984, https://doi.org/10.1021/acs.inorgchem.9b03338.
[108] S.K. Swami, A. Kumar, V. Dutta, Deposition of kesterite Cu_2ZnSnS_4 (CZTS) thin films by spin coating technique for solar cell application, Energy Proc. 33 (2013) 198–202, https://doi.org/10.1016/j.egypro.2013.05.058.
[109] J. Wang, P. Zhang, X. Song, L. Gao, Cu_2ZnSnS_4 thin films: spin coating synthesis and photoelectrochemistry, RSC Adv. 4 (41) (2014) 21318–21324, https://doi.org/10.1039/c4ra01139b.
[110] B. Flynn, W. Wang, C.H. Chang, G.S. Herman, Microwave assisted synthesis of Cu_2ZnSnS_4 colloidal nanoparticle inks, Phys. Status Solidi Appl. Mater. Sci. 209 (11) (2012) 2186–2194, https://doi.org/10.1002/pssa.201127734.
[111] P. Prabeesh, V.G. Sajeesh, I. Packia Selvam, M.S. Divya Bharati, G. Mohan Rao, S.N. Potty, CZTS solar cell with non-toxic buffer layer: a study on the sulphurization temperature and absorber layer thickness, Sol. Energy 207 (April) (2020) 419–427, https://doi.org/10.1016/j.solener.2020.06.103.
[112] M.I. Khalil, R. Bernasconi, A. Lucotti, A. Le Donne, R.A. Mereu, S. Binetti, J.L. Hart, M.L. Taheri, L. Nobili, L. Magagnin, CZTS thin film solar cells on flexible Molybdenum foil by electrodeposition-annealing route, J. Appl. Electrochem. 1 (3) (Nov. 2020), https://doi.org/10.1007/s10800-020-01494-1.
[113] S. Engberg, J. Symonowicz, J. Schou, S. Canulescu, K.M.Ø. Jensen, Characterization of Cu2ZnSnS4 Particles Obtained by the Hot-Injection Method, ACS Omega 5 (18) (2020) 10501–10509. https://doi.org/10.1021/acsomega.0c00657.
[114] R.J. Deokate, R.S. Kate, S.C. Bulakhe, Physical and optical properties of sprayed Cu_2ZnSnS_4 (CZTS) thin film: effect of Cu concentration, J. Mater. Sci. Mater. Electron. 30 (4) (2019) 3530–3538, https://doi.org/10.1007/s10854-018-00630-0.
[115] H. Chen, Q. Ye, X. He, J. Ding, Y. Zhang, J. Han, J. Liu, C. Liao, J. Mei, W. Lau, Electrodeposited CZTS solar cells from Reline electrolyte, Green Chem. 16 (8) (2014) 3841–3845, https://doi.org/10.1039/c4gc00142g.
[116] S.A. Khalate, R.S. Kate, J.H. Kim, S.M. Pawar, R.J. Deokate, Superlattices and Microstructures Effect of Deposition Temperature on the Properties of Cu_2ZnSnS_4 (CZTS) Thin Fi Lms, vol. 103, 2017, https://doi.org/10.1016/j.spmi.2017.02.003.
[117] R.J. Deokate, H.S. Chavan, H. Im, A.I. Inamdar, Spray-deposited kesterite Cu_2ZnSnS_4 (CZTS): optical , structural , and electrical investigations for solar cell applications, Ceram. Int. 48 (1) (2022) 795–802, https://doi.org/10.1016/j.ceramint.2021.09.160.
[118] S.A. Khalate, R.S. Kate, R.J. Deokate, A review on energy economics and the recent research and development in energy and the Cu_2ZnSnS_4 (CZTS) solar cells : a focus towards efficiency, Sol.Energy 169 (May) (2018) 616–633, https://doi.org/10.1016/j.solener.2018.05.036.
[119] N.M. Shinde, R.J. Deokate, C.D. Lokhande, Properties of spray deposited Cu_2ZnSnS_4 (CZTS) thin films, J. Anal. Appl. Pyrolysis 100 (2013) 12–16, https://doi.org/10.1016/j.jaap.2012.10.018.
[120] C.A. Macías-Cabrera, J. Campos-Álvarez, S.A. Gamboa, J.A. Aguilar-Martínez, Y. Peña-Méndez, Synthesis of CZTS thin films from binary precursors stacking by chemical bath deposition for solar cell applications, Mater. Today Proc. 46 (2020) 3109–3113, https://doi.org/10.1016/j.matpr.2021.02.624.
[121] J.O. Jeon, K.D. Lee, L.S. Oh, S.W. Seo, D.K. Lee, H. Kim, J.H. Jeong, M.J. Ko, B. Kim, H.J. Son, J.Y. Kim, Highly efficient copper-zinc-tin-selenide (CZTSe) solar cells by electrodeposition, ChemSusChem 7 (4) (2014) 1073–1077, https://doi.org/10.1002/cssc.201301347.
[122] Y. Li, T. Yuan, L. Jiang, Z. Su, F. Liu, Growth and characterization of Cu_2ZnSnS_4 photovoltaic thin films by electrodeposition and sulfurization, J. Alloys Compd. 610 (2014) 331–336, https://doi.org/10.1016/j.jallcom.2014.05.014.
[123] Q. Guo, G.M. Ford, W.C. Yang, B.C. Walker, E.A. Stach, H.W. Hillhouse, R. Agrawal, Fabrication of 7.2% efficient CZTSSe solar cells using CZTS nanocrystals, J. Am. Chem. Soc. 132 (49) (2010) 17384–17386, https://doi.org/10.1021/ja108427b.
[124] S.C. Riha, B.A. Parkinson, A.L. Prieto, Solution-based synthesis and characterization of Cu_2ZnSnS_4 nanocrystals, J. Am. Chem. Soc. 131 (34) (2009) 12054–12055, https://doi.org/10.1021/ja9044168.
[125] A.D. Collord, H.W. Hillhouse, Composition control and formation pathway of CZTS and CZTGS nanocrystal inks for kesterite solar cells, Chem. Mater. 27 (5) (2015) 1855–1862, https://doi.org/10.1021/acs.chemmater.5b00104.
[126] B.D. Chernomordik, A.E. Beland, N.D. Trejo, A.A. Gunawan, D.D. Deng, K.A. Mkhoyan, E.S. Aydil, Rapid facile synthesis of Cu_2ZnSnS_4 nanocrystals, J. Mater. Chem. 2 (27) (2014) 10389–10395, https://doi.org/10.1039/c4ta01658k.
[127] C. Coughlan, K.M. Ryan, Complete study of the composition and shape evolution in the synthesis of Cu_2ZnSnS_4 (CZTS) semiconductor nanocrystals, CrystEngComm 17 (36) (2015) 6914–6922, https://doi.org/10.1039/c5ce00497g.
[128] W. Wang, M.T. Winkler, O. Gunawan, T. Gokmen, T.K. Todorov, Y. Zhu, D.B. Mitzi, Device characteristics of CZTSSe thin-film solar cells with 12.6% efficiency, Adv. Energy Mater. 4 (7) (2014) 1–5, https://doi.org/10.1002/aenm.201301465.
[129] Gong, Y., Zhu, Q., Li, B., Wang, S., Duan, B., Lou, L., Xiang, C., Jedlicka, E., Giridharagopal, R., Zhou, Y., Dai, Q., Yan, W., Chen, S., Meng, Q., Xin, H.

(2022). Elemental de-mixing-induced epitaxial kesterite/CdS interface enabling 13%-efficiency kesterite solar cells. *Nature Energy* 2022 7:10, 7(10), 966–977. https://doi.org/10.1038/s41560-022-01132-4

[130] Q. Li, A.X. Wei, W.K. Tao, J. Liu, Y. Zhao, Z.M. Xiao, Effect of reaction temperature and reaction time on the properties of Cu_2ZnSnS_4 nanocrystalline thin films prepared by microwave irradiation, Chalcogenide Lett. 14 (11) (2017) 465–474.

[131] P.R. Ghediya, T.K. Chaudhuri, Doctor-blade printing of Cu_2ZnSnS_4 films from microwave-processed ink, J. Mater. Sci. Mater. Electron. 26 (3) (2015) 1908–1912, https://doi.org/10.1007/s10854-014-2628-1.

[132] M. Johnson, S.V. Baryshev, E. Thimsen, M. Manno, X. Zhang, I.V. Veryovkin, C. Leighton, E.S. Aydil, Alkali-metal-enhanced grain growth in Cu_2ZnSnS_4 thin films, Energy Environ. Sci. 7 (6) (2014) 1931–1938, https://doi.org/10.1039/c3ee44130j.

[133] A. Nagaoka, H. Miyake, T. Taniyama, K. Kakimoto, Y. Nose, M.A. Scarpulla, K. Yoshino, Effects of sodium on electrical properties in Cu_2ZnSnS_4 single crystal, Appl. Phys. Lett. 104 (15) (2014), https://doi.org/10.1063/1.4871208, 0-4.

[134] V.V. Satale, S.V. Bhat, Superstrate type CZTS solar cell with all solution processed functional layers at low temperature, Sol. Energy 208 (Sep. 2020) 220–226, https://doi.org/10.1016/j.solener.2020.07.055.

[135] P. Heremans, J. Poortmans, Barry P. Rand, Jan Genoe, Solar cells utilizing small molecular weight organic semiconductors, Prog. Photovoltaics Res. Appl. 15 (2007) 659–676, https://doi.org/10.1002/pip.788.

[136] G.K. Gupta, A. Dixit, Effect of precursor and composition on the physical properties of the low-cost solution processed Cu_2ZnSnS_4 thin film for solar photovoltaic application, J. Renew. Sustain. Energy 9 (1) (2017), https://doi.org/10.1063/1.4974341.

[137] Y. Karzazi, I. Arbouch, Inorganic photovoltaic cells: operating principles, technologies and efficiencies - review, J. Mater. Environ. Sci. 5 (5) (2014) 1505–1515.

[138] M.Z. Klaus Jager, Olindo Isabella, Arno H.M. Smets, A.C.M.M. Rene, Van Swaaij, Solar Energy Fundamentals, Technology and Systems, 2014, pp. 1–401.

[139] S. Das, Growth, Fabrication and Characterization of $Cu_2ZnSn(S_xSe_{1-x})_4$ Photovoltaic Absorber and Thin-Film Heterojunction Solar Cells, 2014.

[140] M. Nanu, J. Schoonman, A. Goossens, Nanocomposite Three-Dimensional Solar Cells Obtained by Chemical Spray Deposition, 2005, https://doi.org/10.1021/nl0509632.

[141] A. Hossein, C. Khavar, A.R. Mahjoub, N. Taghavinia, A. Goossens, J. Hofhuis, Spray-deposited $CuInS_2$ solar cells, IOP Publ. Nanotechnol. Nanotechnol. 19 (2008) 8, https://doi.org/10.1088/0957-4484/19/42/424018.

[142] J.W. Cho, S.J. Park, W. Kim, B.K. Min, Fabrication of nanocrystal ink based superstrate-type $CuInS_2$ thin film solar cells, Nanotechnology 23 (26) (2012), https://doi.org/10.1088/0957-4484/23/26/265401.

[143] D. Lee, K. Yong, Solution-processed Cu_2ZnSnS_4 superstrate solar cell using vertically aligned ZnO nanorods, Nanotechnology 25 (6) (2014), https://doi.org/10.1088/0957-4484/25/6/065401.

[144] M.S. Kumar, S.P. Madhusudanan, S.K. Batabyal, Substitution of Zn in Earth-Abundant $Cu_2ZnSn(S,Se)_4$ based thin film solar cells-A status review, Sol. Energy Mater. Sol. Cells 185 (March) (2018) 287–299, https://doi.org/10.1016/j.solmat.2018.05.003.

[145] S. Varadharajaperumal, C. Sripan, R. Ganesan, G. Hegde, M.N. Satyanarayana, Morphology controlled n-type TiO2 and stoichiometry adjusted p-type Cu_2ZnSnS_4 thin films for photovoltaic applications, Cryst. Growth Des. 17 (10) (2017) 5154–5162, https://doi.org/10.1021/acs.cgd.7b00632.

[146] E. Peksu, H. Karaagac, Preparation of CZTS thin films for the fabrication of ZnO nanorods based superstrate solar cells, J. Alloys Compd. 884 (2021), 161124, https://doi.org/10.1016/j.jallcom.2021.161124.

[147] H. Wang, Progress in thin film solar cells based on Cu_2ZnSnS_4, Int. J. Photoenergy 2011 (2011), https://doi.org/10.1155/2011/801292. Figure 2.

[148] V. Kumar, V.G. Masih, Fabrication and characterization of screen-printed Cu_2ZnSnS_4 films for photovoltaic applications, J. Electron. Mater. 48 (4) (Apr. 2019) 2195–2199, https://doi.org/10.1007/s11664-019-07053-5.

[149] Q. Chen, S. Cheng, S. Zhuang, X. Dou, Cu_2ZnSnS_4 solar cell prepared entirely by non-vacuum processes, Thin Solid Films 520 (19) (2012) 6256–6261, https://doi.org/10.1016/j.tsf.2012.05.074.

[150] K. Tanaka, M. Oonuki, N. Moritake, H. Uchiki, Cu_2ZnSnS_4 thin film solar cells prepared by non-vacuum processing, Sol. Energy Mater. Sol. Cells 93 (5) (2009) 583–587, https://doi.org/10.1016/j.solmat.2008.12.009.

[151] Q.M. Chen, Z.Q. Li, Y. Ni, S.Y. Cheng, X.M. Dou, Doctor-bladed Cu_2ZnSnS_4 light absorption layer for low-cost solar cell application, Chin. Phys. B 21 (3) (Mar. 2012), https://doi.org/10.1088/1674-1056/21/3/038401.

[152] M. Karbassi, S. Baghshahi, N. Riahi- Noori, R. Siavash Moakhar, Deposition of Cu_2ZnSnS_4 films by doctor blade printing using a one-step microwave heated ink as an absorber layer for solar cells, Ceram. Int. 46 (2) (Feb. 2020) 2325–2331, https://doi.org/10.1016/j.ceramint.2019.09.223.

[153] M. Kurokawa, K. Tanaka, K. Moriya, H. Uchiki, Fabrication of three-dimensional-structure solar cell with Cu 2ZnSnS 4, Japanese Journal of Applied Physics 51 (10 PART 2) (2012) 10NC33. https://doi.org/10.1143/JJAP.51.10NC33.

[154] K. Tanaka, M. Kurokawa, K. Moriya, H. Uchiki, Surface morphology improvement of three-dimensional solar cell with Cu_2ZnSnS_4 absorber, J. Alloys Compd. 571 (Sep. 2013) 98–102, https://doi.org/10.1016/j.jallcom.2013.03.060.

[155] M. Berruet, Y. Di Iorio, C.J. Pereyra, R.E. Marotti, M. Vázquez, Highly-efficient superstrate Cu_2ZnSnS_4 solar cell fabricated low-cost methods, Phys. Status Solidi Rapid Res. Lett. 11 (8) (2017) 2–6, https://doi.org/10.1002/pssr.201700144.

[156] V. Najafi, S. Kimiagar, Cd-free Cu_2ZnSnS_4 thin film solar cell on a flexible substrate using nano-crystal ink, Thin Solid Films 657 (Jul. 2018) 70–75, https://doi.org/10.1016/j.tsf.2018.05.013.

[157] M. Zhong, S. Liu, H. Li, C. Li, Superstrate-type Cu_2ZnSnS_4 solar cells without sulfurization fabricated by spray pyrolysis, Chalcogenide Lett. 15 (3) (2018) 133–137.

[158] R.N. Gayen, T. Chakrabarti, Effect of series and shunt resistance on the photovoltaic properties of solution-processed zinc oxide nanowire based CZTS solar cell in superstrate configuration, Mater. Sci. Semicond. Process. 100 (April) (2019) 1–7, https://doi.org/10.1016/j.mssp.2019.04.018.

[159] R. Chen, J. Fan, C. Liu, X. Zhang, Y. Shen, Y. Mai, Solution-Processed one-dimensional ZnO@CdS heterojunction toward efficient Cu_2ZnSnS_4 solar cell with inverted structure, Sci. Rep. 6 (October) (2016) 1–9, https://doi.org/10.1038/srep35300.

[160] J. Kaza, M.R. Pasumarthi, P.S. Avadhani, Superstrate and substrate thin film configuration of CdS/CZTS solar cell fabricated using SILAR method, Opt Laser. Technol. 131 (Nov. 2020) 106413, https://doi.org/10.1016/j.optlastec.2020.106413.

[161] A. Krishnan, K. Rishad Ali, G. Vishnu, P. Kannan, Towards phase pure CZTS thin films by SILAR method with augmented Zn adsorption for photovoltaic applications, Mater. Renew. Sustain. Energy 8 (3) (Sep. 2019) 3, https://doi.org/10.1007/s40243-019-0152-1.

[162] L.M. Peter, Electrochemical routes to earth-abundant photovoltaics: a mini-review, Electrochem. Commun. 50 (2015) 88–92, https://doi.org/10.1016/j.elecom.2014.11.012.

[163] A. Rukini, L. Suhaimi, A.S. Pradhipta, M. Anggara, An analysis of Potential Utilization of Low Cost Cu_2ZnSnS_4 Thin Film Based Photovoltaic in Sumbawa, IOP Conf. Ser.: Earth Environ. Sci. (2013), https://doi.org/10.1088/1755-1315/396/1/012011.

[164] M. Ristov, G. Sinadinovski, I. Grozdanov, Chemical deposition of Cu_2O thin films, Thin Solid Films 123 (1) (Jan. 1985) 63–67, https://doi.org/10.1016/0040-6090(85)90041-0.

[165] Y.F. Nicolau, Solution deposition of thin solid compound films by a successive ionic-layer adsorption and reaction process, Appl. Surf. Sci. 22–23 (PART 2) (May 1985) 1061–1074, https://doi.org/10.1016/0378-5963(85)90241-7.

[166] G. Banerjee, S. Das, S. Ghosh, Optical properties of Cu_2ZnSnS_4 (CZTS) made by SILAR method, in: Materials Today: Proceedings vol. 18, Jan. 2019, pp. 494–500, https://doi.org/10.1016/j.matpr.2019.06.236.

[167] H.M. Pathan, C.D. Lokhande, Deposition of Metal Chalcogenide Thin Films by Successive Ionic Layer Adsorption and Reaction (SILAR) Method, 2004.

[168] G.L. Agawane, S.W. Shin, S.A. Vanalakar, M.P. Suryawanshi, A.V. Moholkar, J.H. Yun, J. Gwak, J.H. Kim, Synthesis of simple, low cost and benign sol–gel Cu_2ZnSnS_4 thin films: influence of different annealing atmospheres, J. Mater. Sci. Mater. Electron. 26 (3) (2015) 1900–1907, https://doi.org/10.1007/s10854-014-2627-2.

[169] X. Song, X. Ji, M. Li, W. Lin, X. Luo, H. Zhang, A review on development prospect of CZTS based thin film solar cells, Int. J. Photoenergy 2014 (2014), https://doi.org/10.1155/2014/613173.

[170] K. Tanaka, N. Moritake, H. Uchiki, Preparation of Cu_2ZnSnS_4 thin films by sulfurizing sol-gel deposited precursors, Sol. Energy Mater. Sol. Cells 91 (13) (Aug. 2007) 1199–1201, https://doi.org/10.1016/j.solmat.2007.04.012.

[171] D. Lee, K. Yong, Superstrate $CuInS_2$ photovoltaics with enhanced performance using a CdS/ZnO nanorod array, ACS Appl. Mater. Interfaces 4 (12) (2012) 6758–6765, https://doi.org/10.1021/am301957d.

[172] W. Yang, H.S. Duan, K.C. Cha, C.J. Hsu, W.C. Hsu, H. Zhou, B. Bob, Y. Yang, Molecular solution approach to synthesize electronic quality Cu_2ZnSnS_4 thin films, J. Am. Chem. Soc. 135 (18) (May 2013) 6915–6920, https://doi.org/10.1021/ja312678c.

[173] N. Yu, R. Zhong, W. Zhong, X. Chen, J. Luo, X. Gu, X. Hu, L. Zhang, J. Hu, Z. Chen, Synthesis of Cu2ZnSnS4 film by air-stable molecular-precursor ink for constructing thin film solar cells, RSC Adv. 4 (68) (2014) 36046–36052, https://doi.org/10.1039/c4ra04363d.

[174] H. Wang, J. Bell, Thin film solar cells based on Cu_2ZnSnS_4 absorber, in: J. Mathew, L. Ma, A. Tan, M. Weijnen, J. Lee (Eds.), Engineering Asset Management and Infrastructure Sustainability, Springer, London, 2012, https://doi.org/10.1007/978-0-85729-493-7_78.

[175] N. Nakayama, K. Ito, Sprayed films of stannite Cu_2ZnSnS_4, Appl. Surf. Sci. 92 (1996) 171–175.

[176] Y.J. Zhu, F. Chen, Microwave-assisted preparation of inorganic nanostructures in liquid phase, Chem. Rev. 114 (12) (2014) 6462–6555, https://doi.org/10.1021/cr400366s.

[177] A.H. Pinto, S.W. Shin, E. Isaac, T.R. Knutson, E.S. Aydil, R.L. Penn, Controlling Cu_2ZnSnS_4 (CZTS) phase in microwave solvothermal synthesis, J. Mater. Chem. 5 (44) (2017) 23179–23189, https://doi.org/10.1039/c7ta06086f.

[178] S.M. Robati, M. Imani, A. Tadjarodi, Ultrafast synthesis of crystalline Cu_2ZnSnS_4 nanoparticles by solid state microwave heating technique and study of their electrochemical behavior, Mater. Lett. 225 (2018) 9–12, https://doi.org/10.1016/j.matlet.2018.04.085.

[179] K.C. Wang, P. Chen, C.M. Tseng, Facile one-pot synthesis of Cu2ZnSnS4 quaternary nanoparticles using a microwave-assisted method, CrystEngComm 15 (46) (2013) 9863–9868. https://doi.org/10.1039/c3ce41691g.

[180] K.C. Wang, P. Chen, C.M. Tseng, Facile one-pot synthesis of Cu_2ZnSnS_4 quaternary nanoparticles using a microwave-assisted method, CrystEngComm 15 (46) (2013) 9863–9868, https://doi.org/10.1039/c3ce41691g.
[181] V.A. Madiraju, K. Taneja, M. Kumar, R. Seelaboyina, CZTS synthesis in aqueous media by microwave irradiation, J. Mater. Sci. Mater. Electron. 27 (4) (2016) 3152–3157, https://doi.org/10.1007/s10854-015-4137-2.
[182] D.B. Mitzi, O. Gunawan, T.K. Todorov, K. Wang, S. Guha, The path towards a high-performance solution-processed kesterite solar cell, Sol. Energy Mater. Sol. Cells 95 (6) (2011) 1421–1436, https://doi.org/10.1016/j.solmat.2010.11.028.
[183] R. Saravana Kumar, C.H. Hong, M.D. Kim, Doughnut-shaped hierarchical Cu_2ZnSnS_4 microparticles synthesized by cyclic microwave irradiation, Adv. Powder Technol. 25 (5) (2014) 1554–1559, https://doi.org/10.1016/j.apt.2014.05.005.
[184] H. Yang, X. Su, A. Tang, Microwave synthesis of nanocrystalline Sb_2S_3 and its electrochemical properties, Mater. Res. Bull. 42 (7) (2007) 1357–1363, https://doi.org/10.1016/j.materresbull.2006.10.002.
[185] C. Wang, C. Cheng, Y. Cao, W. Fang, L. Zhao, X. Xu, Synthesis of Cu_2ZnSnS_4 nanocrystallines by a hydrothermal route, Jpn. J. Appl. Phys. 50 (6 PART 1) (2011) 4–7, https://doi.org/10.1143/JJAP.50.065003.
[186] R. Saravana Kumar, B.D. Ryu, S. Chandramohan, J.K. Seol, S.K. Lee, C.H. Hong, Rapid synthesis of sphere-like Cu_2ZnSnS_4 microparticles by microwave irradiation, Mater. Lett. 86 (2012) 174–177, https://doi.org/10.1016/j.matlet.2012.07.059.
[187] S.W. Shin, J.H. Han, C.Y. Park, S.R. Kim, Y.C. Park, G.L. Agawane, A.V. Moholkar, J.H. Yun, C.H. Jeong, J.Y. Lee, J.H. Kim, A facile and low cost synthesis of earth abundant element Cu_2ZnSnS_4 (CZTS) nanocrystals: effect of Cu concentrations, J. Alloys Compd. 541 (2012) 192–197, https://doi.org/10.1016/j.jallcom.2012.06.086.
[188] W. Tao, A. Wei, Y. Zhao, J. Liu, Z. Xiao, Effect of solution concentration on the properties of Cu_2ZnSnS_4 nanocrystalline thin films prepared by microwave irradiation, J. Mater. Sci. Mater. Electron. 28 (4) (2017) 3407–3414, https://doi.org/10.1007/s10854-016-5936-9.
[189] W. Wang, H. Shen, F. Jiang, X. He, Z. Yue, Low-cost chemical fabrication of Cu_2ZnSnS_4 microparticles and film, J. Mater. Sci. Mater. Electron. 24 (6) (2013) 1813–1817, https://doi.org/10.1007/s10854-012-1017-x.
[190] B. Patro, S. Vijaylakshmi, P. Sharma, Effect of different sulphur precursors on morphology and band-gap on the formation of Cu_2ZnSnS_4 (CZTS) particles with microwave irradiation, AIP Conf. Proc. 1731 (2016) 2–5, https://doi.org/10.1063/1.4948221.
[191] F. Long, S. Chi, J. He, J. Wang, X. Wu, S. Mo, Z. Zou, Synthesis of hexagonal wurtzite Cu_2ZnSnS_4 prisms by an ultrasound-assisted microwave solvothermal method, J. Solid State Chem. 229 (2015) 228–234, https://doi.org/10.1016/j.jssc.2015.06.012.
[192] W. Wang, H. Shen, X. He, Study on the synthesis and formation mechanism of Cu_2ZnSnS_4 particles by microwave irradiation, Mater. Res. Bull. 48 (9) (2013) 3140–3143, https://doi.org/10.1016/j.materresbull.2013.04.078.
[193] Y. Zhao, W. Tao, X. Chen, J. Liu, A. Wei, Synthesis and characterization of Cu_2ZnSnS_4 nanocrystals prepared by microwave irradiation method, J. Mater. Sci. Mater. Electron. 26 (8) (2015) 5645–5652, https://doi.org/10.1007/s10854-015-3114-0.
[194] Y. Zhao, W. Tao, J. Liu, A. Wei, Rapid synthesis of Cu_2ZnSnS_4 nanocrystalline thin films directly on transparent conductive glass substrates by microwave irradiation, Mater. Lett. 148 (2015) 63–66, https://doi.org/10.1016/j.matlet.2015.02.068.
[195] B. Patro, S. Vijaylakshmi, R.K. Reddy, P. Sharma, Microwave-assisted solvothermal synthesis of Cu_2ZnSnS_4 (CZTS) nanocrystals for photovoltaic applications, Mater. Today Proc. 3 (8) (2016) 2786–2794, https://doi.org/10.1016/j.matpr.2016.06.028.
[196] L. Arora, P. Gupta, N. Chhikara, P. Singh, N. Muhunthan, V.N. Singh, B.P. Singh, K. Jain, S. Chand, Green Synthesis of Wurtzite Copper Zinc Tin Sulfide Nanocones for Improved Solar Photovoltaic, Utilization, Appl. Nanosci. (2016), https://doi.org/10.1007/s13204-014-0302-9.
[197] A.H. Pinto, S.W. Shin, A. Sharma, R.L. Penn, E.S. Aydil, Synthesis of $Cu_2(Zn_{1-x}Co_x)SnS_4$ nanocrystals and formation of polycrystalline thin films from their aqueous dispersions, J. Mater. Chem. 6 (3) (2018) 999–1008, https://doi.org/10.1039/c7ta06295h.
[198] A. Ghosh, S. Palchoudhury, R. Thangavel, Z. Zhou, N. Naghibolashrafi, K. Ramasamy, A. Gupta, A new family of wurtzite-phase Cu_2ZnAS_{4-x} and $CuZn_2AS_4$ (A = Al, Ga, In) nanocrystals for solar energy conversion applications, Chem. Commun. 52 (2) (2016) 264–267, https://doi.org/10.1039/c5cc07743e.
[199] C. Ma, H. Guo, K. Zhang, N. Yuan, J. Ding, Fabrication of p-type kesterite Ag_2ZnSnS_4 thin films with a high hole mobility, Mater. Lett. 186 (October 2016) (2017) 390–393, https://doi.org/10.1016/j.matlet.2016.10.013.
[200] T. Gokmen, O. Gunawan, T.K. Todorov, D.B. Mitzi, Band tailing and efficiency limitation in kesterite solar cells, Appl. Phys. Lett. 103 (10) (2013) 2–7, https://doi.org/10.1063/1.4820250.
[201] G. Zhong, K. Tse, Y. Zhang, X. Li, L. Huang, C. Yang, J. Zhu, Z. Zeng, Z. Zhang, X. Xiao, Induced effects by the substitution of Zn in Cu_2ZnSnX_4 (X = S and Se), Thin Solid Films 603 (2016) 224–229, https://doi.org/10.1016/j.tsf.2016.02.005.
[202] R.R. Prabhakar, S. Zhenghua, Z. Xin, T. Baikie, L.S. Woei, S. Shukla, S.K. Batabyal, O. Gunawan, L.H. Wong, Photovoltaic effect in earth abundant solution processed Cu_2MnSnS_4 and $Cu_2MnSn(S,Se)_4$ thin films, Sol. Energy Mater. Sol. Cells 157 (2016) 867–873, https://doi.org/10.1016/j.solmat.2016.07.006.